Altered allostery of the left flipper domain underlies the weak ATP response of rat P2X5 receptors

Received for publication, June 28, 2019, and in revised form, November 12, 2019 Published, Papers in Press, November 14, 2019, DOI 10.1074/jbc.RA119.009959

Liang-Fei Sun[‡1], Yan Liu[‡1], Jin Wang[‡1], Li-Dong Huang[‡], Yang Yang[‡], Xiao-Yang Cheng[‡], Ying-Zhe Fan[§], Michael X. Zhu[¶], Hong Liang[‖], Yun Tian[**], Heng-Shan Wang[‖2], Chang-Run Guo[‡‡3], and Ye Yu[‡**‡‡4]

*From the [‡]Institute of Medical Sciences and Department of Pharmacology and Physiology, Shanghai Jiao Tong University School of Medicine, Shanghai 200025, China, the [‖]State Key Laboratory for Chemistry and Molecular Engineering of Medicinal Resources, School of Chemistry and Pharmacy, Guangxi Normal University, Guilin, 541004, China, the [‡‡]Department of Basic Medicine and Clinical Pharmacy, China Pharmaceutical University, Nanjing 210009, China, the [¶]Department of Integrative Biology and Pharmacology, McGovern Medical School, University of Texas Health Science Center, Houston, Texas 77030, the **College of Bioscience and Biotechnology, Hunan Agricultural University, Changsha 410128, China, and the [§]Putuo District Center Hospital, Shanghai University of Chinese Traditional Medicine, Shanghai 200026, China*

Edited by Roger J. Colbran

Although the extracellular ATP-gated cation channel purinergic receptor P2X5 is widely expressed in heart, skeletal muscle, and immune and nervous systems in mammals, little is known about its functions and channel-gating activities. This lack of knowledge is due to P2X5's weak ATP responses in several mammalian species, such as humans, rats, and mice. WT human P2X5 (hP2X5$^{\Delta 328-349}$) does not respond to ATP, whereas a full-length variant, hP2X5 (hP2X5-FL), containing exon 10 encoding the second hP2X5 transmembrane domain (TM2), does. However, although rat P2X5 (rP2X5) has a full-length TM2, ATP induces only weak currents in rP2X5, which prompted us to investigate the mechanism underlying this small ATP response. Here, we show that single replacements of specific rP2X5 residues with the corresponding residues in hP2X5 (S191F or F195H) significantly enhance the current amplitude of rP2X5. Using a combination of engineered disulfide cross-linking, single-channel recording, and molecular modeling, we interrogated the effects of S191F and F195H substitutions on the allostery of the left flipper (LF) domain. On the basis of our findings, we propose that the bound ATP-induced distinct allostery of the LF domain with that of other functional subtypes has caused the weak ATP response of rP2X5 receptors. The findings of our study provide the prerequisite for future transgenic studies on the physiological and pathological functions of P2X5 receptors.

This study was supported by Guangxi Funds for Distinguished Experts, National Natural Science Foundation of China, Grants 31971146, 81603409, 31971042, 21977021, 31900808, 31570832, 31170787, 31400707, and 81703677; National Postdoctoral Program for Innovative Talents Grant BX201700306; China Postdoctoral Science Foundation Grant 2018M632127; the Project Program of the State Key Laboratory of Natural Medicines of China Pharmaceutical University; National Program on Key Basic Research Project of China Grant 2014CB910300/02; National Excellent Young Scientist Foundation of China Grant 31222018; Hunan Provincial Natural Science Foundation of China Grant 2018JJ1012; and Science and Technology Department of Hunan Province Grant 2018RS3086. The authors declare that they have no conflicts of interest with the contents of this article.

[1] These authors contributed equally to this work.
[2] To whom correspondence may be addressed. Tel.: 86-21-6445-3296; Fax: 86-21-6445-3296; E-mail: hshwang2002@163.com.
[3] To whom correspondence may be addressed. Tel.: 86-21-6445-3296; Fax: 86-21-6445-3296; E-mail: crguocpu@126.com.
[4] To whom correspondence may be addressed. Tel.: 86-21-6445-3296; Fax: 86-21-6445-3296; E-mail: yuye@shsmu.edu.cn.

As a class of trimeric extracellular ATP-gated ion channels permeable to cations, Na^+, K^+, and Ca^{2+}, P2X receptors are implicated in a variety of physiological and pathological processes (1–5). Several small molecules targeting P2X receptors, like AF-219 (phase III), have entered into clinical trials (6, 7), signifying the potential of these channels as the new drug targets. So far, seven P2X genes, encoding P2X1–7 subtypes, have been cloned from both excitable (such as neurons and muscle cells) and nonexcitable (like platelets and endothelial cells) cells, where they form both homomeric and heteromeric P2X receptor complexes (8–11). The different P2X subtypes expressed in various tissues have been implicated in diverse physiological and pathological processes (3, 4).

Compared with other functional subtypes, current knowledge about P2X5 is relatively limited (4). First cloned from rat celiac ganglia, P2X5 was later found in mesencephalic nucleus, heart, and spinal cord (11). Although ATP and its analog 2-Me-S-ATP could activate P2X5, with the concentration of ATP evoking half-maximum currents through P2X receptors (EC_{50}) reaching ~10–50 μM, the current amplitudes of homomeric P2X5 from several mammalian species, including humans, mice, and rats, were strikingly small as compared with that generated by other P2X subtypes (11–14). This is true for currents recorded in both primary cells and cell lines with P2X5 overexpression. The fact that the *P2X5* gene was not lost during evolution or did not become a pseudogene, like *TRPC2* (15), implies that this P2X subtype plays important roles in physiological and/or pathological processes. Indeed, P2X5 has been implicated in cell fate determination of myocutaneous cells (16) and sensitizing acid pain evoked by lactic acid during exercises (17). Also, the expression of P2X5 is up-regulated in polycystic kidney disease (18). Furthermore, P2X5 and P2X7 receptors have been shown to be colocalized in squamous epithelial cell layers, participating in cell proliferation to differentiation (19). Additionally, heteromeric P2X1/5 (20–22) receptors are involved in neuropathic pain (23) and Ca^{2+} signaling in cortical

astrocytes (24). Functional evidence for the existence of heteromeric P2X2/5 receptors was also obtained recently (25). Therefore, homomeric or heteromeric P2X5 receptors may participate in a variety of physiological and pathological processes. However, many questions still remain unanswered, including 1) whether or not the small sustained current induced by ATP is responsible for the P2X5-mediated pathophysiological functions mentioned above, 2) whether P2X5 functions mainly through forming heterotrimers with other P2X subunits, and 3) whether homomeric P2X5 can produce sizable currents under certain conditions, such as specific developmental stages. Gene sequencing at the different developmental stages and transgenic studies could provide some clues for clarifying these questions. In the meantime, elucidating the mechanism underlying the weak ATP response of homomeric mammalian P2X5 receptors and identifying functional variants, especially in model animals like rats and mice, would advance our understanding of P2X5 gating and contribute to future functional studies of P2X5 using transgenic animals.

It has been demonstrated that polymorphism in exon 10 of the human *P2X* gene is responsible for the loss-of-function of hP2X5 receptors (13). Kotnis *et al.* (14) cloned a full-length hP2X5 (hP2X5-FL), which is present only in a small population of African Americans. hP2X5-FL contains an intact exon 10, which encodes the second transmembrane (TM2)[5] domain of this receptor, and is able to develop a large current in response to extracellular ATP. However, even with the presence of the full-length TM2, rP2X5 still exhibited weak ATP response. In the present study, we sought to uncover the reason for the discrepancy between the nonfunctional rP2X5 and the functional hP2X5-FL. We constructed a series of chimeras between the two P2X5 receptors for functional evaluation and identified two residues in the left flipper (LF) domain as responsible for the lack of function of rP2X5. As revealed by cysteine cross-linking, single-channel recordings, histidine protonation and deprotonation, and molecular dynamics (MD) simulations, the bound ATP cannot induce allosteric changes in the LF domain like other functional P2X subtypes, which leads to a significant decrease in the open probability of rP2X5, and thus, the weak response to ATP.

Results

The chimera with the rP2X5 sequence Val^{171}–Lys^{205} swapped by that of hP2X5-FL enhances the ATP-evoked response

Because the common hP2X5 variant lacking exon 10 (hP2X5$^{\Delta 328-349}$) and rP2X5 produce little or negligible sustained ATP-evoked currents (11, 26), but the full-length hP2X5 (hP2X5-FL, created by inserting exon 10 into hP2X5$^{\Delta 328-349}$) becomes functional (Fig. 1*A*), we constructed 10 chimeras (Fig. 1, *B–D*), namely chimera 1 (CH1) to chimera 10 (CH10), with the following rP2X5 sequences replaced by the corresponding regions of hP2X5-FL: 1–30, 31–50, 51–114, 115–170, 171–205, 206–230, 231–279, 280–341, 342–362, and 363–455, respectively. Among all of these chimeras, only rP2X5^{CH3} and rP2X5^{CH5} acquired sizable responses to ATP (100 μM), with the maximal current densities reaching 72.4 ± 10.8 and 162.0 ± 20.6 pA/pF, respectively (Fig. 1, *C* and *D*), which are much larger than the ATP response of WT rP2X5 (2.02 ± 0.77 pA/pF). Between the two chimeras, only the current character of rP2X5^{CH5} is comparable with that of hP2X5-FL (Fig. 1*C*).

To examine whether the lack or gain of the ATP responses of the chimeras could result from altered protein surface expression, we assessed the membrane surface and total protein levels by a cell-surface biotinylation assay and Western blotting. Although reduced surface expressions were detected for several chimeras, the reduction was not large enough to account for the lack of ATP responses of some of these chimeras except for CH4 (Fig. 1, *E* and *F*). The unchanged or slightly reduced surface expressions of rP2X5^{CH5} and rP2X5^{CH3} further suggest that trafficking deficit could not be the cause for the absence of ATP responses of WT rP2X5 (Fig. 1, *E* and *F*) and that the replaced amino acid sequences are responsible for increasing the channel function of rP2X5^{CH5} and rP2X5^{CH3}.

Single substitutions (S191F and F195H) significantly increase the ATP-evoked response of rP2X5

We focused on rP2X5^{CH5} in subsequent experiments. This chimera contains amino acids 171–205 of hP2X5, which differs from Val^{171}–Lys^{205} of rP2X5 by 10 residues (Fig. 2*A*). To identify the key residues involved in ATP activation in this region, we made a series of rP2X5 constructs containing individual substitutions of the 10 residues with the corresponding one from hP2X5-FL. Whole-cell recordings revealed that two of the single amino acid substitutions, S191F and F195H, markedly enhanced the ATP-evoked currents of rP2X5, with the maximal current densities (I_{max}) reaching 99.3 ± 2.2 and 143.0 ± 19.6 pA/pF, respectively (Fig. 2, *B* and *C*), whereas other substitutions displayed no or very small (L181F, 18.8 ± 5.0 pA/pF) ATP-induced currents (Fig. 2, *B* and *C*).

Based on the crystal structures of zebrafish P2X4 (zfP2X4) receptors (27, 28), we created the homology models of rP2X5. The homology model of rP2X5 at the open state revealed a possible direct interaction between Ser^{191} and ATP (Fig. 2*D*). Therefore, the Ser → Phe substitution at Ser^{191} may increase the affinity to ATP and thereby restore the rP2X5 response to ATP. Indeed, as revealed by the concentration-response curves, the apparent affinity of rP2X5^{S191F} to ATP was increased by >20-fold when compared with that of rP2X5^{WT} (EC_{50} = 26.8 ± 13.9 and 0.96 ± 0.31 μM, for WT and S191F, respectively; Fig. 2*E*). However, even with 20 mM ATP, the current generated by rP2X5^{WT} was negligibly small (Fig. 2*B*), suggesting that the increased apparent affinity to ATP was not the only reason for the enhancement of ATP response in rP2X5^{S191F}. On the other hand, Phe^{195} is not located within the ATP-binding pocket of rP2X5 (Fig. 2*D*), but the Phe → His substitution (rP2X5^{F195H}) still exhibited an increased ATP response (Fig. 2, *B* and *C*). Interestingly, rP2X5^{F195H} had a slightly decreased, rather than increased, apparent affinity to ATP (EC_{50} = 45.4 ± 2.0 μM; Fig. 2*E*) as compared with rP2X5^{WT}, further supporting our speculation. Furthermore,

[5] The abbreviations used are: TM2, second transmembrane; LF, left flipper; DF, dorsal fin; MD, molecular dynamics; pF, picofarads; r.m.s., root mean square; H-bond, hydrogen bond; β-ME, β-mercaptoethanol; nAChR, nicotinic acetylcholine receptor; ASIC3, acid-sensing ion channel 3; HEK-293, human embryonic kidney 293; GAPDH, glyceraldehyde-3-phosphate dehydrogenase; HRP, horseradish peroxidase; COM, center of mass; ANOVA, analysis of variance; AMPA, α-amino-3-hydroxy-5-methyl-4-isoxazolepropionic acid; EGFP, enhanced GFP; CH1–CH10, chimeras 1–10, respectively.

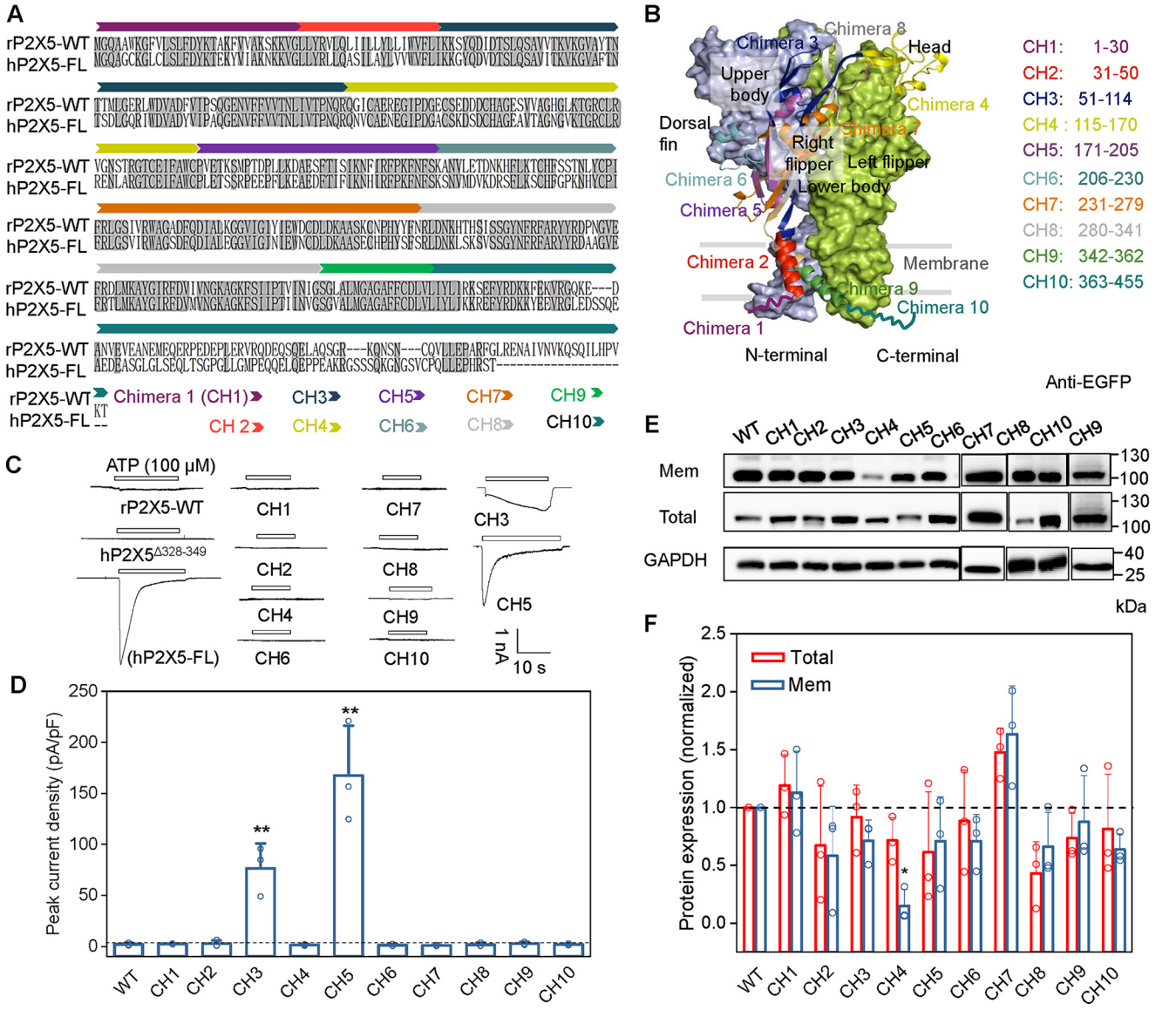

Figure 1. Strategies for chimera constructions and representative recordings of rP2X5^{WT}, hP2X5-FL, and chimeras. *A*, *schematic diagram* of chimera constructions based on the sequences of rP2X5^{WT} and hP2X5-FL. The rP2X5 chimeras were generated by replacing certain regions of rP2X5^{WT} with corresponding sequences of hP2X5-FL. *B*, *different colors* indicate different regions of rP2X5 in one chain replaced by the corresponding sequences of hP2X5-FL. The other two chains are displayed in *calamine blue* and *grass green* surfaces for emphasis. *C* and *D*, representative current traces (*C*) and maximal ATP responses (*D*) of 10 chimeras (pA/pF, 100 μM, mean ± S.D. (*error bars*), $n = 3–4$). *, $p < 0.05$; **, $p < 0.01$ *versus* WT, one-way ANOVA with Bonferroni post hoc test ($F(10, 31) = 51.57$, $p < 0.0001$). *C*, *schematic diagram* indicates gain-of-function chimeras CH3(51–114) and CH5(171–205). *E* and *F*, representative Western blotting (*E*) and mean values (*F*) of the membrane and total expressions of rP2X5 WT and chimeras transfected in HEK-293 cells. At least three experiments were performed: *, $p < 0.05$; **, $p < 0.01$ *versus* WT, one-way ANOVA with Bonferroni post hoc test ($F(10, 22) = 4.209$, $p = 0.0024$ and $F(10, 22) = 5.523$, $p = 0.0004$, for total and surface expressions, respectively).

there was no significant difference in the cell-surface expression of S191F and F195H as compared with WT rP2X5 (Fig. 2, *G* and *I*), and increasing the amount of rP2X5^{WT} cDNA in the transfection (6 μg) failed to improve the ATP response (Fig. 2*C*). Therefore, we postulated that the S191F and F195H substitutions might have elevated the ATP response of rP2X5 by altering the channel gating, rather than increasing the protein expression.

To further evaluate the effects of these residues on channel gating of P2X5, we replaced Phe^{191} and His^{195} of hP2X5-FL with the corresponding residues of rP2X5, namely hP2X5-FL^{F191S} and hP2X5-FL^{H195F}. The substitution of F191S, but not of H195F, noticeably decreased the maximal ATP response of hP2X5-FL (I_{max} = 39.2 ± 9.9 pA/pF for hP2X5-FL^{F191S} and 278.0 ± 52.8 pA/pF for hP2X5-FL^{H195F}; Fig. 2*F*). Both mutants showed a slight decrease in cell-surface expression, but such a decrease is unlikely to account for the large reduction in the current density of hP2X5-FL^{F191S}, especially given that despite the similar decrease in surface expression, hP2X5-FL^{H195F} exhibited similar current density as hP2X5-FL^{WT} (Fig. 2, *H* and *J*). Altogether, these results suggest that Ser^{191} is mainly responsible for the extremely small ATP-evoked current of rP2X5 receptors.

The gain-of-function of rP2X5^{S191F} may result from an altered allostery of the LF domain

In the homology model of rP2X5, the residue at position 191 makes direct interactions with ATP (Fig. 3*A*). Structural

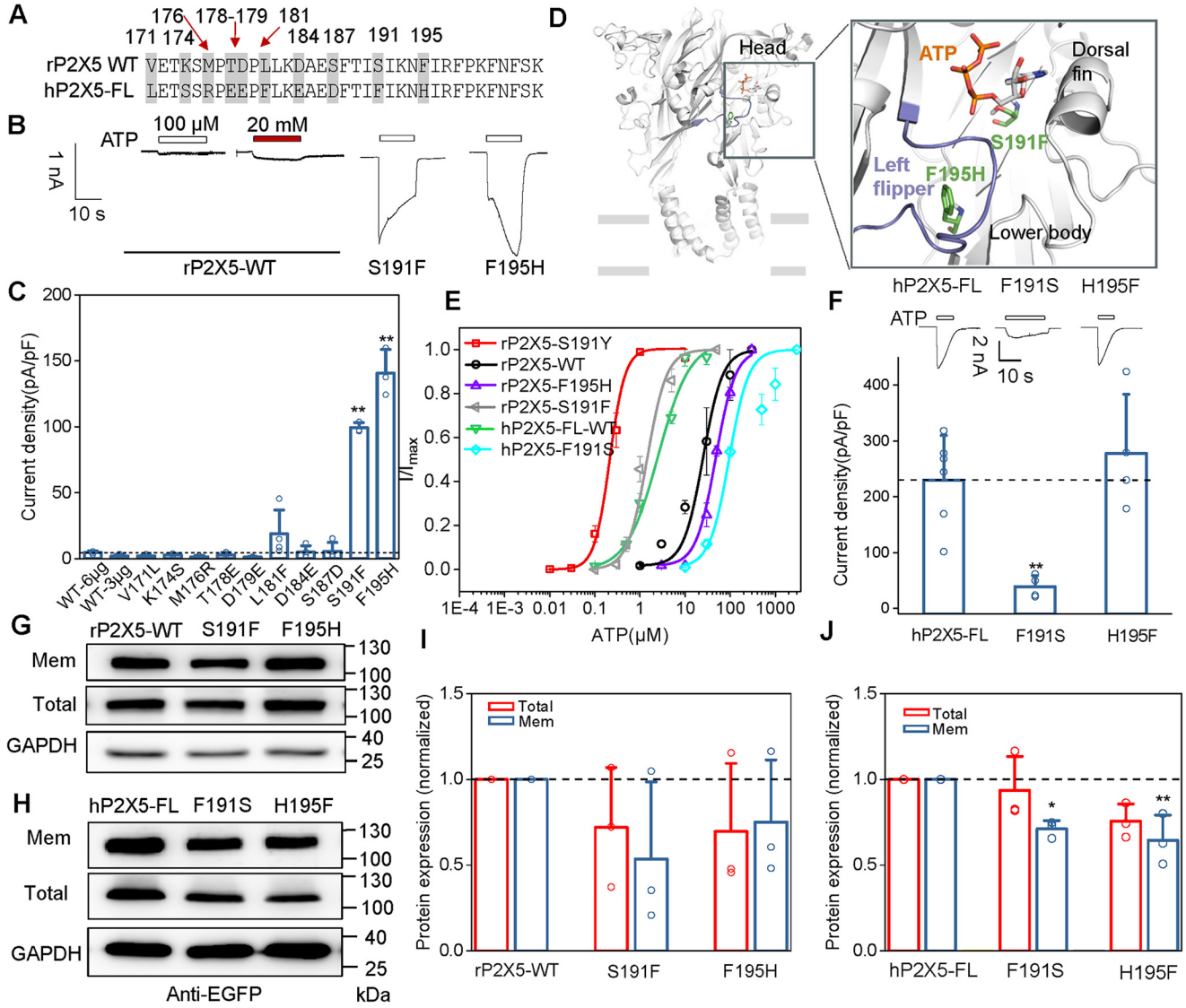

Figure 2. Single amino acid replacement (S191F or F195H) remarkedly enhances the ATP response of rP2X5. *A*, sequence alignment of the segment 171–205 in rP2X5-WT and hP2X5-FL, with amino acid residues different between $rP2X5^{WT}$ and hP2X5-FL *labeled* in *gray*. *B* and *C*, representative current traces (*B*) and pooled data (*C*; mean ± S.D. (*error bars*), $n = 3–4$) of $rP2X5^{S191F}$, $rP2X5^{F195H}$, and $rP2X5^{WT}$ induced by 100 μM ATP or 20 mM ATP. *, $p < 0.05$; **, $p < 0.01$ *versus* WT, one-way ANOVA with Bonferroni post hoc test ($F(10, 30) = 113.7$, $p < 0.0001$). *D*, *zoom-in view* of the constructed model of rP2X5 based on the open structure of zfP2X4 to illuminate the location of sites Ser^{191} and Phe^{195}. *E*, concentration-response curves of rP2X5 and its mutants (mean ± S.E. (*error bars*), $n = 3–5$). Each *solid line* is a fit of the Hill equation to the ATP-dependent activation. *F*, typical recordings (*top*) and pooled data (*bottom*) of hP2X5-FL and its mutants induced by 100 μM ATP (mean ± S.D. (*error bars*), $n = 4–6$). *, $p < 0.05$; **, $p < 0.01$ *versus* WT, one-way ANOVA with Bonferroni post hoc test ($F(2, 11) = 10.87$, $p = 0.0025$). *G–J*, representative Western blotting (*G* and *H*) and mean values (*I* and *J*) of protein expressions of $rP2X5^{WT}$ and its mutants (*G* and *I*) and hP2X5-FL and its mutants (*H* and *J*) transfected in HEK-293 cells. At least three experiments were performed. *, $p < 0.05$; **, $p < 0.01$ *versus* WT, one-way ANOVA with Bonferroni post hoc test (pooled data in *I*, $F(2, 6) = 0.2886$ ($p = 0.7591$) and $F(2, 6) = 1.052$ ($p = 0.4059$) for total and surface expressions, respectively; data in *J*, $F(2, 6) = 6.948$ ($p = 0.0274$) and $F(2, 6) = 1.063$ ($p = 0.4025$) for total and surface expressions, respectively).

dynamic comparisons between $rP2X5^{WT}$ and $rP2X5^{S191F}$ using MD simulations followed by ligand root mean square (r.m.s.) fluctuation analysis revealed that the triphosphate groups (atoms 1–10) and the purine ring (atoms 20–30) of ATP were more stable in $rP2X5^{S191F}$ than in $rP2X5^{WT}$ (Fig. 3, *B* and *C*), probably because the phenylalanine at this position makes more contacts with ATP (Fig. 3*D*, *middle*). By contrast, a serine in the same position dramatically reduced the interaction between ATP and rP2X5 (Fig. 3*D*, *top*). Further analysis showed that the introduction of phenylalanine significantly enhanced the hydrophobic interaction between $rP2X5^{S191F}$ and ATP (Fig. 3*E*, *middle*). As revealed by a saturation-mutation screening of Ser^{191}, in a certain range, along with the increase in the steric hindrance of the side chain, the response to ATP approached closer and closer to that of $hP2X5\text{-}FL^{WT}$ (I_{max} = 23.3 ± 1.6, 69.1 ± 15.1, 99.3 ± 2.24, and 369 ± 31 pA/pF, for S191L, S191M, S191F, and S191Y, respectively; Fig. 3, *F* and *G*). Nevertheless, an oversized steric hindrance may also be unfavorable, such as S191W (Fig. 3, *F* and *G*). As for S191P, the imino group in the proline side chain made it unable to form the β-fold and consequently resulted in a functional loss (Fig. 3*G*). Other amino acid substitutions did not significantly increase the ATP response of rP2X5 (Fig. 3, *F* and *G*), probably due to the altered shape and hydrophobic/hydrophilic properties of the ATP-binding pocket (like S191E/D/K/R/H) or improper/insufficient contacts with ATP (such as S191G/C/T/N/Q/V/I).

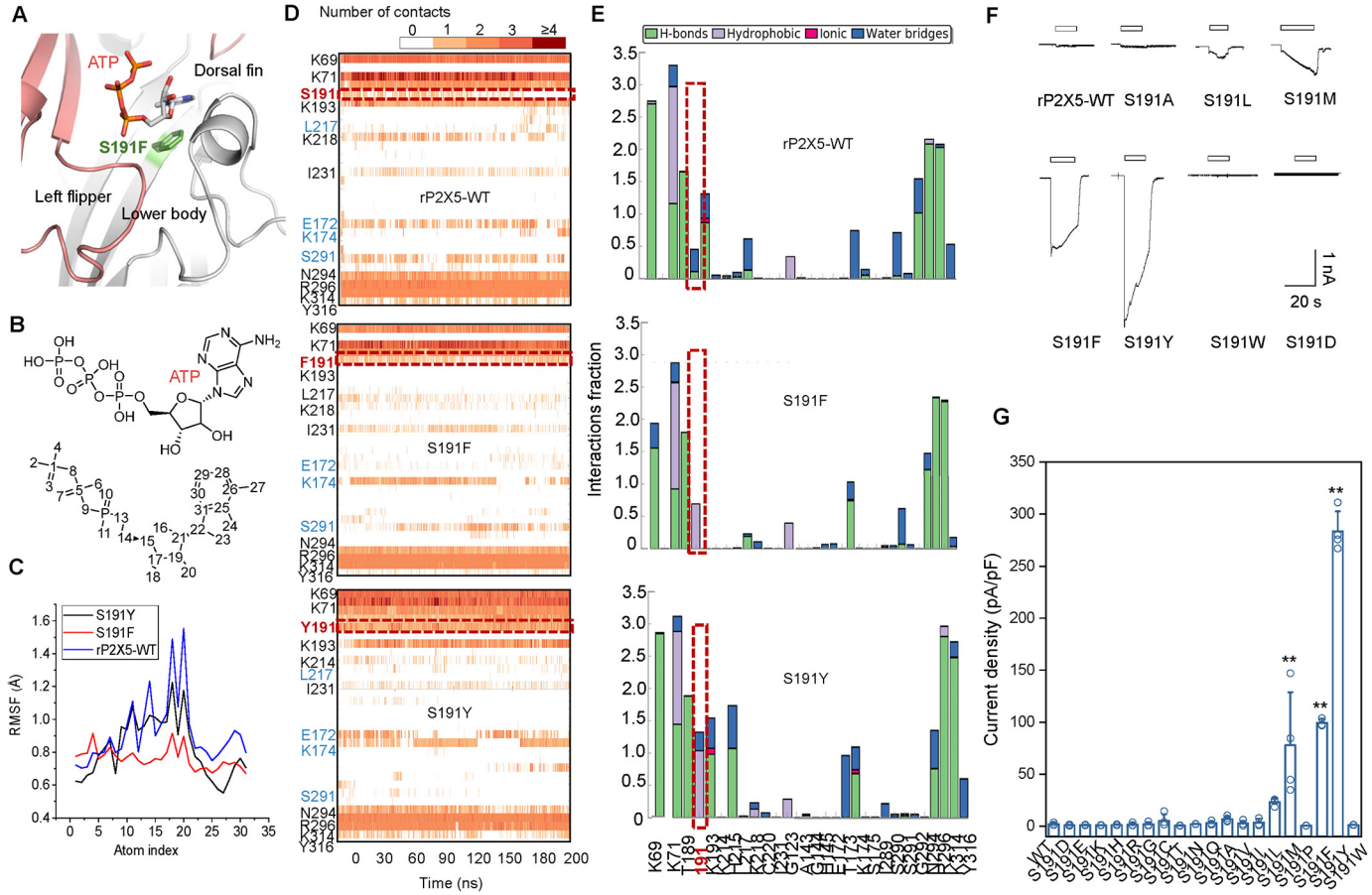

Figure 3. Phenylalanine or tyrosine introduced at position 191 produces additional contacts with the bound ATP. *A*, *zoom-in view* of the constructed model of rP2X5^{S191F} based on the open structure of zfP2X4. *B* and *C*, r.m.s fluctuation analysis of each atom (*C*) and of ATP when it binds to rP2X5^{WT} or rP2X5^{S191F} and rP2X5^{S191Y} (*B*). *D*, *timeline representations* of the P2X5 WT– or mutant–ATP interactions and contacts, including H-bonds and hydrophobic, ionic, and water bridge interactions. Some residues producing more than one specific contact with the ATP are represented by a *darker shade* of *orange*. *E*, P2X5-ATP interactions monitored throughout the simulations of rP2X5^{WT}, rP2X5^{S191F}, or rP2X5^{S191Y}. *F* and *G*, representative current traces and pooled data (mean ± S.E. (*error bars*), $n = 3–4$) of rP2X5^{WT} and mutations with substitutions in site Ser^{191} for hydrophobic residues activated by 100 μM ATP (*F*). *, $p < 0.05$; **, $p < 0.01$ *versus* WT, one-way ANOVA with Bonferroni post hoc test ($F(19, 53) = 31.77$, $p < 0.0001$).

Because 20 mM ATP could not effectively activate rP2X5^{WT} (Fig. 2*B*), the enhanced channel function of rP2X5^{S191F} cannot be simply attributed to the increased ATP affinity. Based on the crystal structures of P2X4 and P2X3 receptors at both open and closed states (27–29), we have previously demonstrated that the relative motions of the LF and DF domains induced by ATP, namely the downward movement of the LF domain and the upward movement of the DF domain, play a vital role in the channel activation of P2X receptors (30, 31). In addition, the downward motion of the LF domain facilitates the intersubunit physical coupling, which transmits ATP binding to channel gating of P2X receptors (32). Therefore, we built homology models of rP2X5^{WT}, rP2X5^{S191F}, and rP2X5^{S191Y} at both the *apo*/closed and open states and examined the effects of S191F and S191Y substitutions on the motions of LF and DF domains as well as channel gating. As revealed by these models, phenylalanine at site 191 makes more hydrophobic interactions than serine with the residues of the DF (Ile^{231} and Leu^{217}), lower body (Ile^{289} and the aliphatic chain of Lys^{193}), and LF domains (Val^{208}), which may promote the final conformational changes in those domains (Fig. 4*A*). Expectedly, MD simulation analysis of rP2X5^{WT} and rP2X5^{S191F} showed that S191F evoked significant conformation changes of the LF and DF domains at the *apo*/closed state, especially for the LF domain (Fig. 4*B*). Comparing C_α–C_α distances among 191 ··· Ile^{289} ··· Lys^{214} (Fig. 4, *B* and *C*) and pair distributions of the distance of center of mass (COM) among the LF, DF, and β2-sheet (in the lower body domain) (Fig. 4*D*) during MD simulations of rP2X5^{WT} and rP2X5^{S191F}, we found that Phe^{191} more effectively pushed the LF domain away from the ATP-binding pocket than Ser^{191} (Fig. 4, *B–E*). Meanwhile, the DF domain migrated slightly outward and eventually shortened its distance from the LF domain (Fig. 4, *B–E*). These Phe^{191}-induced alterations in the conformation of rP2X5 are in line with the conformational changes required for channel gating after ATP binding (Fig. 4*A*), implying that Phe^{191} may facilitate the LF domain to prime channel gating of rP2X5^{S191F}. We also performed additional MD simulations on rP2X5^{S191Y} and found that the bulkier side chain of Tyr^{191} produced even more contacts with ATP than Phe^{191} (Fig. 3, *D* and *E*, *bottom panels*), including stronger hydrophobic and water-aided hydrogen-bond (H-bond) interactions. These interactions led to ~10-fold increase in the apparent affinity to ATP (Fig. 2*E*). The additional contacts also led to altered conformation of the LF and DF domains both at the resting (Fig. 4, *D* and *E*) and open states for rP2X5^{S191Y} (Fig. 3, *D* and *E*, *bottom panels*), indicating that the increased ATP response of S191Y pos-

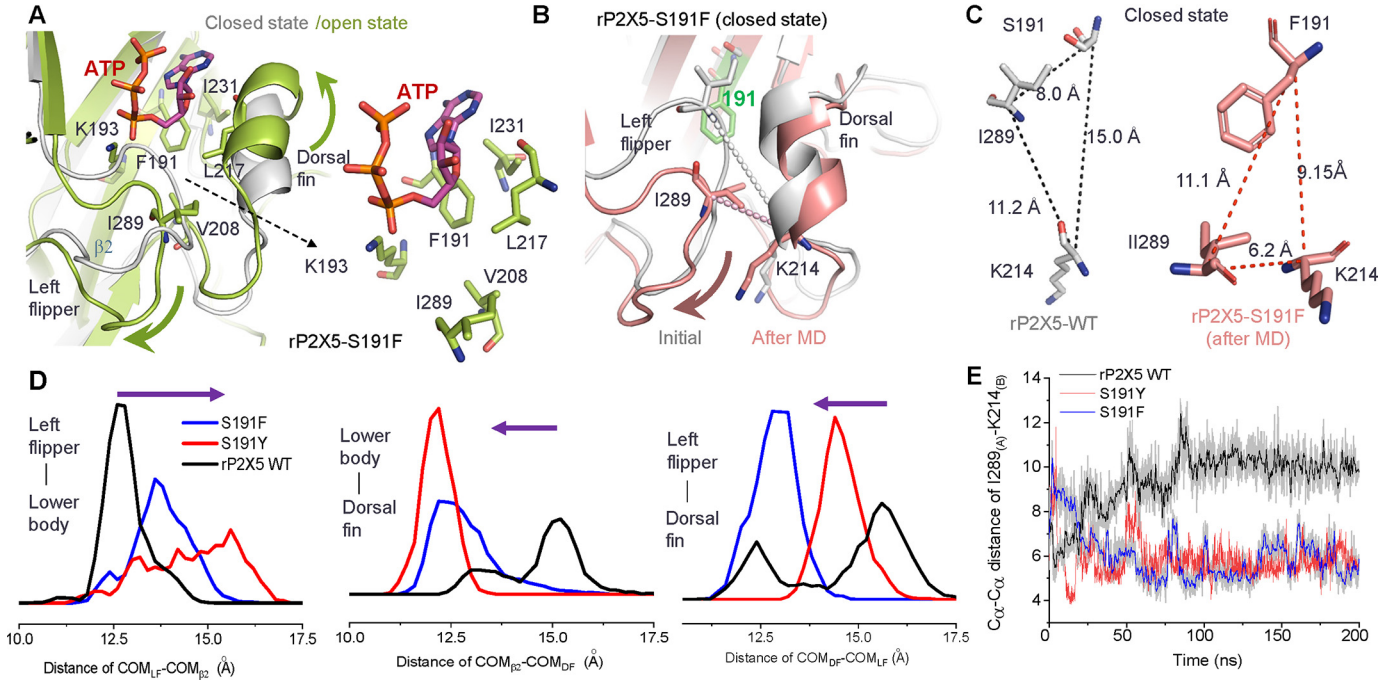

Figure 4. Introduction of phenylalanine or tyrosine at position 191 could induce significant conformational changes of the LF domain. *A, zoom-in view* of the superimposed homology models of P2X5^{S191F} in the closed and open states. Introduced phenylalanine at the position 191 produced more contacts with the hydrophobic residues of the DF (Leu^{217}), lower-body (Lys^{193}), and LF (Ile^{231}) domains. *B–F*, MD simulations of rP2X5^{WT}, rP2X5^{S191F}, and rP2X5^{S191Y} at the resting state. A timeline measurement of C_α–C_α distances between Lys^{214} and Ile^{289} (*E*) and pair distance distributions of the COM between the LF and β2-sheet, β2-sheet and LF, and LF and DF of rP2X5^{WT}, rP2X5^{S191F}, and rP2X5^{S191Y} (*D*) at resting state suggests that the LF domain is repelled outward (*B*) after 200-ns MD simulations.

sibly resulted from some different allosteric changes of the LF and DF domains as compared with that induced by S191F.

We further tested the idea that S191F and S191Y resulted in conformational changes of the LF and DF domains by using an engineered disulfide cross-linking approach (33) (Fig. 5*A*). As revealed by the MD simulations, if the LF domain was pushed outward by Phe^{191} (Fig. 5*B*), the C_α–C_α distance between Ile^{289} (in the LF domain) and Lys^{214} (in the DF domain) would become much closer (from 11.2 to 6.2 Å; Fig. 4, *C* and *E*), making the formation of the intersubunit disulfide bond possible. The MD simulations of the rP2X5$^{S191F/K214C/I289C}$ cross-linking model revealed that the dihedral angle $\chi_{C\beta\text{-}S\gamma\text{-}S\gamma\text{-}C\beta}$ of this engineered disulfide bond was near 91° (Fig. 5, *A* and *B*), a typical dihedral angle for a disulfide bond in proteins (33). These predictions suggest that, compared with rP2X5$^{K214C/I289C}$, it would be easier to detect disulfide bond formation in rP2X5$^{S191F/K214C/I289C}$. Indeed, the protein band representing the trimeric receptors, which requires the formation of intersubunit disulfide bonds, was significantly increased in immunoblots of lysates from cells that expressed rP2X5$^{S191F/K214C/I289C}$ (Fig. 5, *C* and *D*). This band was reduced to the monomeric size by the treatment of β-mercaptoethanol (β-ME, 1%), demonstrating the disulfide cross-linking between the subunits (Fig. 5*C*). Meanwhile, under reducing conditions, the total protein levels (reduced into monomers) of rP2X5$^{K214C/I289C}$ and rP2X5$^{S191F/K214C/I289C}$ were not significantly different (Fig. 5, *C* and *E*), indicating that the increase in the trimeric rP2X5$^{S191F/K214C/I289C}$ was not due to nonspecific aggregation, which could occur because of excessive overexpression. Similar results were also observed in the mutant rP2X5$^{S191Y/K214C/I289C}$ (Fig. 5, *C–E*).

Therefore, S191F or S191Y substitution significantly altered the conformations of LF and DF domains of rP2X5. Because the LF domain is a flexible loop, whereas the DF domain is a rigid α-helix (Figs. 3*A* and 4*B*), Phe^{191} might exert more influence on the LF domain, which primes it to the conformation required for channel gating at the apo-state. This point is further supported by MD simulations (Fig. 4, *B–E*). Moreover, Phe^{191} could make direct hydrophobic contacts with residues of the DF, LF, and lower-body domains (Fig. 4*A*), and the bound ATP could further promote the relative motions of the LF and DF domains through its direct interaction with Phe^{191} (Fig. 4*A*). We have previously suggested that the interdomain hydrophobic interactions among the LF, DF, and lower-body domains pose an energy barrier for channel gating (31), and allosteric events that alter the hydrophobic interactions, with concomitant coordinated motions of LF and DF domains, are essential for channel gating of P2X4 receptors (30). Accordingly, the weak ATP response of rP2X5 may be attributed to the high energy barrier (30) for the channel gating of WT rP2X5 because its LF domain is deeply buried into the ATP-binding pocket. Thus, the alterations in the conformations of LF and DF domains, especially for the LF domain, introduced by S191F possibly decreased the energy barrier of channel gating and thereby resulting in the larger ATP response.

The increased current amplitude of rP2X5^{F195H} is attributed to additional interactions between His^{195} and the LF domain

Additionally, the functional restoration of rP2X5^{F195H} could also be attributed to an altered conformation of the LF domain. Although phenylalanine and histidine possess similar-size side

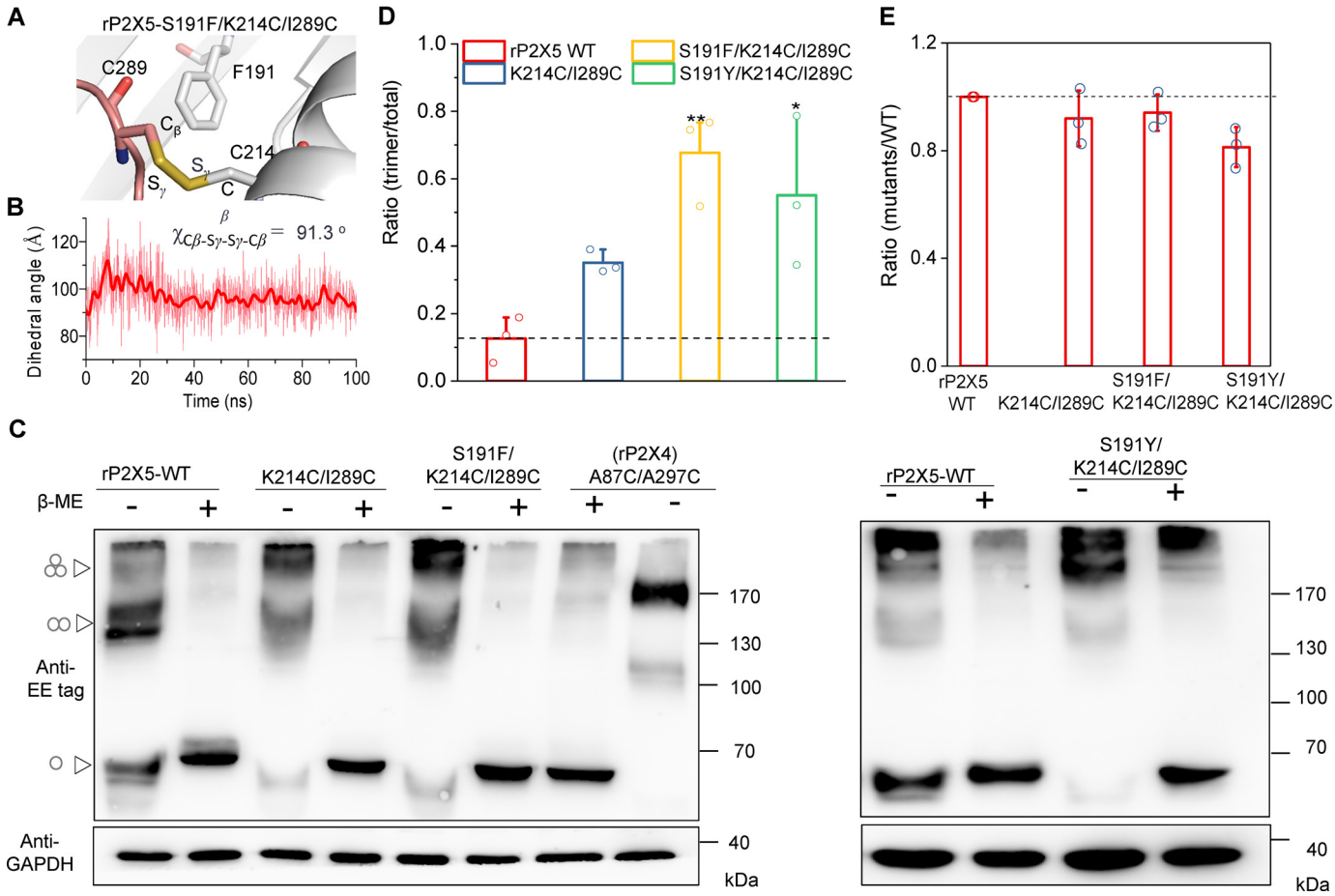

Figure 5. Disulfide cross-linking confirms the distinct conformations of the LF and DF domains in rP2X5^{WT}, rP2X5^{S191F}, and rP2X5^{S191Y}. *A* and *B*, *zoom-in view* of the constructed model of rP2X5$^{S191F/K214C/I289C}$ (*A*) and a timeline measurement of the dihedral angel C_β-S_γ-S_γ-C_β during MD simulations. *C* and *D*, nonreducing Western blotting (*C*) and pooled data (*D*) (mean ± S.D. (*error bars*)) support the formation of intersubunit disulfide bonds between K214C (in the DF domain of one subunit) and I289C (in the LF domain of another subunit) in rP2X5^{WT}, rP2X5^{S191F}, and rP2X5^{S191Y}. Another disulfide cross-linking rP2X4$^{A87C/A297C}$ was shown as control. The molecular mass markers are shown on the *right*, whereas the positions parallel to monomeric, dimeric, and trimeric receptors are indicated by *triangle arrows* on the *left*. Similar results were obtained in at least three independent experiments. *, $p < 0.05$; **, $p < 0.01$ *versus* WT (*dashed line*), one-way ANOVA with Bonferroni post hoc test ($F(3, 8) = 9.339$, $p = 0.0054$). *E*, mean values of the total expressions of rP2X5 WT and mutants transfected in HEK-293 cells. At least three independent experiments were performed: one-way ANOVA with Bonferroni post hoc test ($F(3, 8) = 3.513$, $p = 0.069$).

chains (Fig. 6*A*), the introduction of histidine in rP2X5^{F195H} brings two nitrogen atoms into the side chain, which would facilitate the formation of an H-bond with other residues (Fig. 6*A*). Given that His^{195} is surrounded by nonpolar residues Val^{67}, Ala^{65}, and Ala^{206} in the lower-body domain (Fig. 6*B*), we could exclude the possibility that His^{195} directly interacts with these residues through an H-bond. Therefore, the gain-of-function of rP2X5^{F195H} most likely resulted from polar contacts between the side chain of His^{195} (imidazole ring) and the LF domain (Fig. 6*C*). We performed MD simulations of rP2X5^{F195H} under the conditions with or without bound ATP (Fig. 6*D*). Further H-bond interaction analysis between His^{195} and residues of the LF domain in rP2X5^{F195H} suggested that His^{195} could produce more H-bond contacts with residues of the LF domain when ATP binds to rP2X5 (Fig. 6*D*), indicating that His^{195} mainly contributes to the conformational change of the LF domain at the open state instead of the resting state.

To test this hypothesis, we performed alanine-scanning mutagenesis in the LF domain of rP2X5^{F195H} to identify residues that may produce additional contacts with the imidazole ring of His^{195}. Indeed, F195H/S291A and F195H/G292A exhibited a complete loss of the ATP current of F195H ($I_{max} = 7.03 \pm 1.15$ and 1.48 ± 0.34 pA/pF for F195H/S291A and F195H/G292A, respectively; Fig. 6, *E* and *F*), whereas F195H/D282A ($I_{max} = 59.0 \pm 11.3$ pA/pF) and F195H/T286A ($I_{max} = 94.2 \pm 12.8$ pA/pF) had partially decreased ATP-induced currents compared with rP2X5^{F195H}. Thus, the increased current amplitude of rP2X5^{F195H} relied on the interactions between His^{195} and residues in the LF domain, including Asp^{282}, Thr^{286}, Ser^{291}, and Gly^{292}, especially Ser^{291} and Gly^{292} (Fig. 6*C*). Importantly, equivalent mutations added on rP2X5^{S191F} (rP2X5$^{S191F/S291A}$ and rP2X5$^{S191F/G292A}$) and hP2X5-FL^{WT} (hP2X5-FL^{S291A} and hP2X5-FL^{G292A}) did not affect the maximal ATP responses of the respective receptors (Fig. 6*G*), indicating that the interactions are specific to His^{195} and Ser^{291}/Gly^{292}-mediated functional restoration of rP2X5^{F195H}.

To further examine whether histidine interacts with the LF domain through its nitrogen atoms in the imidazole ring of rP2X5^{F195H}, we changed the pH value of bath solutions. The maximal ATP-evoked current of rP2X5^{F195H} was significantly reduced ($I_{9.0}/I_{7.4} = 0.38 \pm 0.05$, $p < 0.01$, $n = 4$) in the alkaline environment (pH 9.0) but unaffected (pH 6.0) or slightly

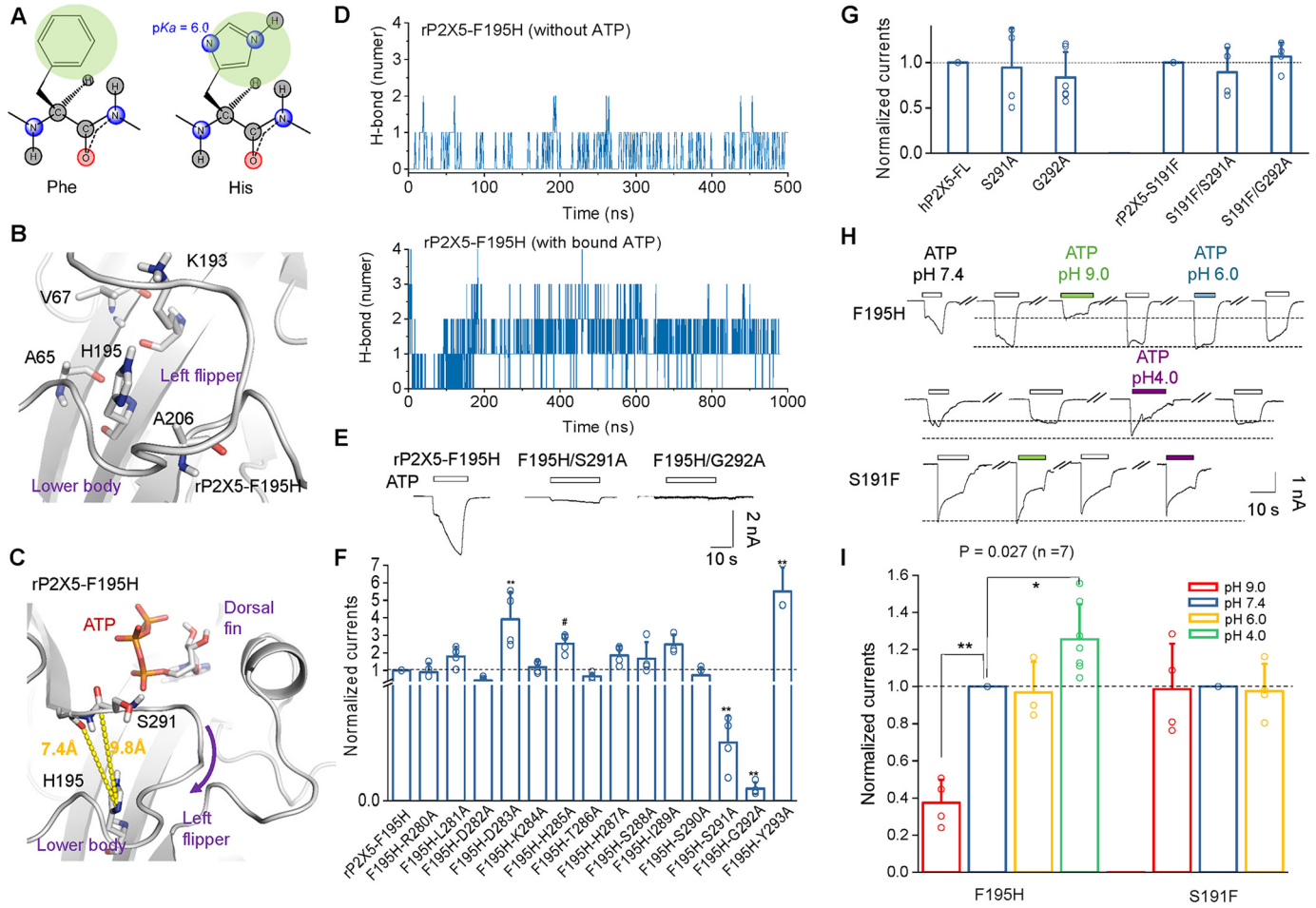

Figure 6. The gain-of-function of F195H is also attributed to altered allostery of the LF domain. *A*, two-dimensional structures of phenylalanine (*left*) and histidine (*right*). The pK_a value of the nitrogen atom, being much closer to the carbon atom of the main chain, in the imidazole ring is 6.0, and this atom can act as either donor or acceptor of H-bonding contacts in different pH values. *B* and *C*, *zoom-in view* of the homology models of rP2X5^{F195H}. Introduced His^{195} is surrounded by a series of nonpolar amino acids (*B*). The distances from the oxygen atoms of Ser^{291} and Gly^{292} to the nitrogen of His^{195} are 9.8 and 7.4 Å, respectively, if ATP does not repel the LF domain out of the ATP-binding pocket. Those distances might be shortened significantly once the channel is opening after the H-bonding contacts are established between His^{195} and Ser^{291} or Gly^{292}. *D*, total number of H-bonds between His^{195} and residues of the LF domain detected in rP2X5^{F195H} during MD simulations. *E* and *F*, representative current traces (*E*) and pooled data (*F*) (mean ± S.D. (*error bars*), $n = 3–5$) of rP2X5^{F195H}, rP2X5$^{F195H/S191A}$, and rP2X5$^{F195H/G292A}$. *, $p < 0.05$; **, $p < 0.01$ *versus* WT, one-way ANOVA with Bonferroni post hoc test ($F(14, 44) = 18.45$, $p < 0.0001$). *G*, summarized effects of mutations S291A and G292A on maximal ATP-evoked currents of hP2X5-FL and rP2X5^{S191F} (mean ± S.D. (*error bars*), $n = 4–6$). *, $p < 0.05$; **, $p < 0.01$ *versus* WT (*dashed line*), one-way ANOVA with Bonferroni post hoc test ($F(2, 11) = 0.4043$ ($p = 0.6769$) and $F(2, 9) = 0.9454$ ($p = 0.4240$) for hP2X5 and rP2X5). *H* and *I*, representative current traces (*H*) and mean values (*I*) (mean ± S.D. (*error bars*), $n = 3–7$) of rP2X5^{F195H} and rP2X5^{S191F} induced by 100 μM ATP in acidic (pH 6.0 or 4.0) and basic (pH 9.0) bath solutions ($F(3, 15) = 35.50$ ($p < 0.0001$) and $F(2, 9) = 0.02126$ ($p = 0.9790$) for F195H and S191F, respectively).

increased (pH 4.0) in the acidic pH (Fig. 6, *H* and *I*), suggesting that His^{195} needs to be protonated to form H-bonds with the oxygen atoms of the main chain of Gly^{292} or Ser^{291}. In addition, according to the homology model of rP2X5^{F195H} at the closed state, the distances between the nitrogen atom of His^{195} (pK_a = 6.0; Fig. 6*A*, *right*) and the oxygen atom of Gly^{292} or Ser^{291} were 7.4 and 9.8 Å, respectively (Fig. 6*C*). During the gating process, these distances will be shortened to 3.0–3.5 Å when H-bonds His^{195}-N$\cdots$H$\cdots$O-Gly^{292}/Ser^{291} were formed (Fig. 6*C*). The H-bond contact would therefore facilitate the downward motion of the LF domain. The fact that the ATP response of rP2X5^{F195H} could be increased to a level similar to that of hP2X5-FL also suggests a lack or much weaker allosteric change of the LF domain during the channel gating of rP2X5^{WT}. Moreover, pH variations did not affect the activation of rP2X5^{S191F} (Fig. 6, *G* and *H*), indicating that the H-bond contact His^{195}-N$\cdots$H$\cdots$O-Gly^{292}/Ser^{291} may be a mechanism specific for the functional restoration of rP2X5^{F195H}.

The increase in the current amplitude of chimera CH3 relies on a residue substitution located under the LF domain

To understand the molecular basis for the partial gain-of-function of the chimera CH3, the 10 discrepant residues in the sequence (residues 51–114) of rP2X5 were individually replaced by their corresponding residues in hP2X5-FL (Fig. 7, *A* and *B*). Among the 10 residue substitutions, only mutation rP2X5^{V67I} could increase the ATP response of rP2X5 (I_{max} = 28.6 ± 4.35 pA; Fig. 7, *C* and *D*). The surface expression of rP2X5^{V67I} was slightly down- rather than up-regulated (Fig. 7, *E* and *F*), indicating that the partially increased channel function was not due to the altered surface expression of rP2X5^{V67I}. Interestingly, differing only by one methyl group, the substitu-

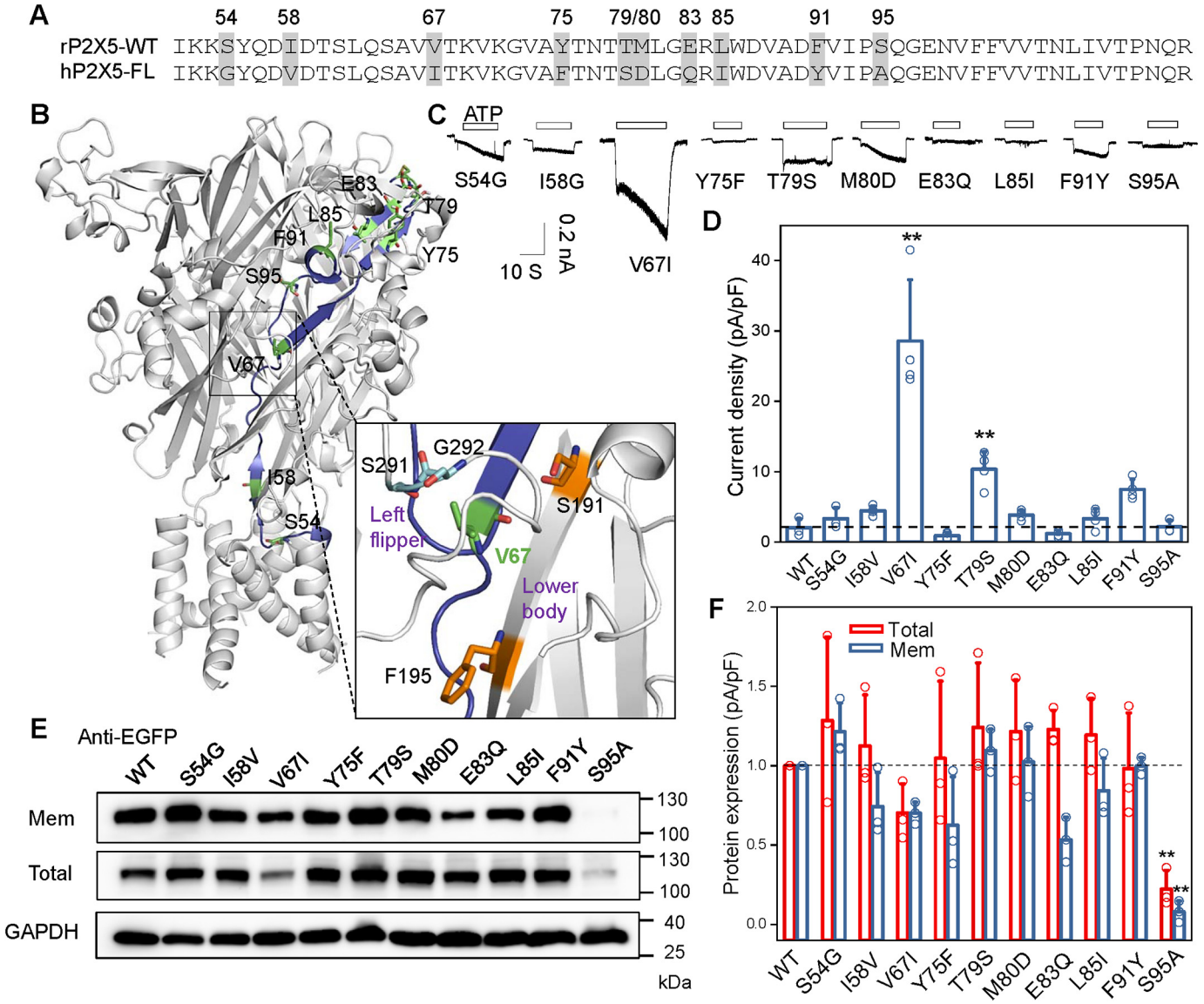

Figure 7. Partial gain-of-function of CH3 is attributed to a single-residue substitution located under the LF domain. *A*, sequence alignment of the segment 171–205 in rP2X5^{WT} and hP2X5-FL, with residues different between rP2X5^{WT} and hP2X5-FL *highlighted* in *gray*. *B*, mapping the sequence differences between the segment 171–205 of rP2X5^{WT} and hP2X5-FL in the homology model rP2X5^{WT} at the resting state, and *zoom-in view* of the site around Val^{67}. Val^{67} is very close to residues Ser^{291} and Gly^{292}. *C* and *D*, representative current traces (*C*) and pooled data (*D*) (mean ± S.D. (*error bars*), $n = 3$–4) of rP2X5^{WT} and its mutants transfected in HEK-293 cells. *, $p < 0.05$; **, $p < 0.01$ *versus* WT (*dashed line*), one-way ANOVA with Bonferroni post hoc test ($F(10, 30) = 27.31$, $p < 0.0001$). *E* and *F*, representative Western blotting (*E*) and mean values (*F*) (mean ± S.D. (*error bars*), $n = 3$) of the membrane and total expressions of rP2X5^{WT} and its mutants transfected in HEK-293 cells. Similar results were obtained from at least three independent experiments. *, $p < 0.05$; **, $p < 0.01$ *versus* WT (*dashed line*), one-way ANOVA with Bonferroni post hoc test ($F(10, 22) = 6.181$ ($p = 0.0002$) and $F(10, 22) = 5.596$ ($p = 0.0004$) for total and surface expressions, respectively).

tion of Val^{67} for isoleucine, which is located under the LF domain (Fig. 7*B*), significantly increased the ATP-evoked current of rP2X5. This may be due to the slightly increased steric hindrance that facilitates the repulsion of the LF domain after ATP binding, like the effect induced by S191F. Moreover, given that Ile^{67} is adjacent to Gly^{292} and Ser^{291} (Fig. 7*B*, *bottom*), it may have a similar effect as His^{195}, pushing Ser^{291}–Gly^{292} away from the ATP-binding pocket after ATP binding. Despite the difference among the mechanisms underlying the increased channel functions of S191F, F195H, and V67I, one thing is clear, that all three mutations more or less modulate the conformation of the LF domain. These mutations either force the LF domain to stay away from the ATP-binding pocket at the resting state or facilitate the LF domain to move away from the pocket after ATP binding. In other words, the ATP binding to rP2X5^{WT} could not effectively cause the LF domain to move downward, a motion essential for the conformational transition from the ATP-binding pocket to the channel pore; therefore, rP2X5 receptors exhibit little or no response to ATP.

The proper conformational changes of the LF domain in rP2X5^{S191F} or rP2X5^{S191Y} allow normal state transition from resting to open and finally desensitization

Finally, to examine the influence of the normal allostery of the LF domain on channel gating of rP2X5, we compared the single-channel currents between rP2X5^{S191F} and rP2X5^{WT}.

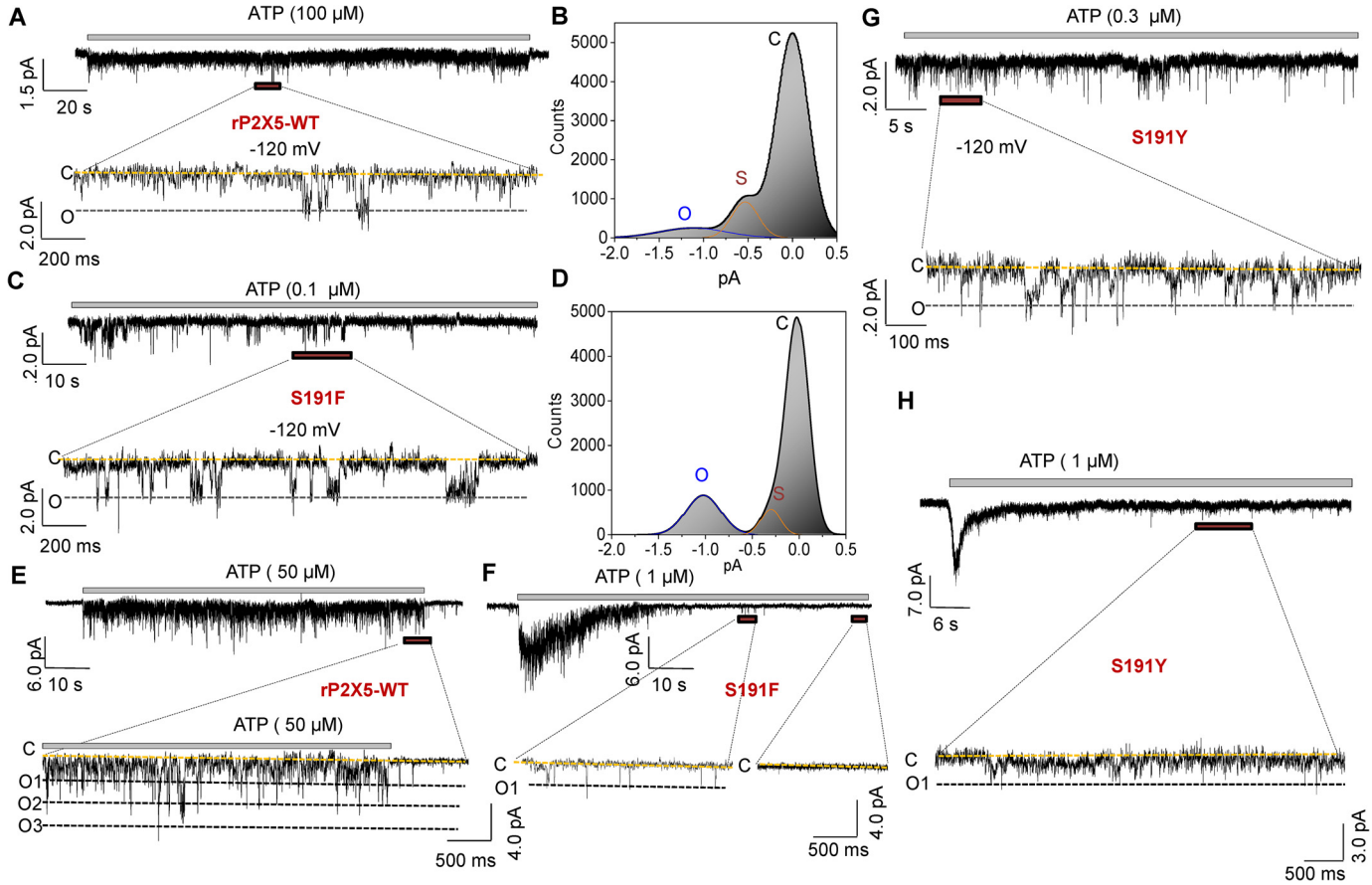

Figure 8. S191F and S191Y increase the opening probability of rP2X5 and promote the state transitions from closed to open and final desensitization. *A–D*, single-channel currents recorded from outside-out patches at −120 mV responses to 100 μM ATP for the rP2X5^{WT} (*A* and *B*), and 0.1 μM ATP for the rP2X5^{S191F} (*C* and *D*). Full opening (*O*) and closing (*C*) are indicated by *black* and *yellow lines*, respectively. *B* and *D*, all-points histograms fitted to the sum of two Gaussians for rP2X5^{WT} (*B*) and rP2X5^{S191F} (*D*). The *y* axis denotes the ratio of the number of events to the number of bins (the bin number is set to 320). *E* and *F*, responses of the rP2X5^{WT} (*E*) and rP2X5^{S191F} (*F*) to ATP (50 and 1 μM for rP2X5^{WT} and rP2X5^{S191F}, respectively) recorded by outside-out macro patch at −120 mV. *G* and *H*, single-channel (*G*) and macroscopic (*H*) patches recorded at −120 mV responses to ATP in rP2X5^{S191Y}. Similar results were obtained from three additional individual patches.

Currents from outside-out patches revealed that saturated ATP concentrations could induce the opening of rP2X5^{WT}, with the majority of the open channels under the subconductance states (<0.6 pA, −120 mV) (Fig. 8, *A* and *B*). In contrast, most rP2X5^{S191F} channels were at a completely opened state in the presence of saturating ATP (~1.0–1.2 pA, −120 mV; Fig. 8, *C* and *D*). Moreover, the single-channel conductance of rP2X5^{S191F} is not different from that of that full open state of rP2X5^{WT} (~10–11 picosiemens), indicating that the conformational changes of the LF domain facilitates the transitions of the channel states, rather than affecting the unitary conductance, which may be attributable to the fact that the LF domain is located far away from the ion permeation pathway (34).

In addition, by macroscopic outside-out patch recordings of rP2X5^{WT} (Fig. 8*E*), we found that although the number of open channels was low, this number was kept stable even after 1-min application of ATP (50 μM), indicating that there were no or only a small proportion of channels that underwent desensitization after a long exposure to ATP. By contrast, the macroscopic patch recordings of rP2X5^{S191F} (Fig. 8*F*) revealed that as low as 1 μM ATP instantaneously activated most of the channels in the patch, but 90% of them desensitized at ~1–1.5 s after the ATP application, and all channels desensitized at ~3–5 s after the ATP application. Therefore, S191F-induced conformational changes of the LF domain can effectively increase the open possibility of rP2X5, by promoting the state transitions from rest to open and finally to desensitization states (Fig. 9). Any factor that impedes this allosteric process would reduce the probability of the channels becoming fully open, trapping them in various subconductance states, as in the case of rP2X5^{WT} (Fig. 8*A*). Similar results were also observed in both micro- and macroscopic outside-out patches of rP2X5^{S191Y} (Fig. 8, *G* and *H*).

Discussion

P2X receptors are trimeric channels activated by extracellular ATP. They are involved in various physiological and pathological processes. Despite the wide expression of P2X5 in several systems, little is known regarding its gating properties and functions, partially due to the extremely small responses of several cloned mammalian P2X5 receptors to ATP. Here, we generate a series of rP2X5 chimeras containing a certain region of the hP2X5-FL sequence and examined their ATP responses, aiming to uncover the mechanisms underlying the weak ATP-evoked currents of rP2X5. Our results revealed that two rP2X5 chimeras, CH3 and CH5, produced significant ATP-evoked currents. Subsequent single-residue substitution experiments identified two key residues (Ser^{191} and Phe^{195}) that are responsible for the weak responses of rP2X5 to ATP. Both S191F and

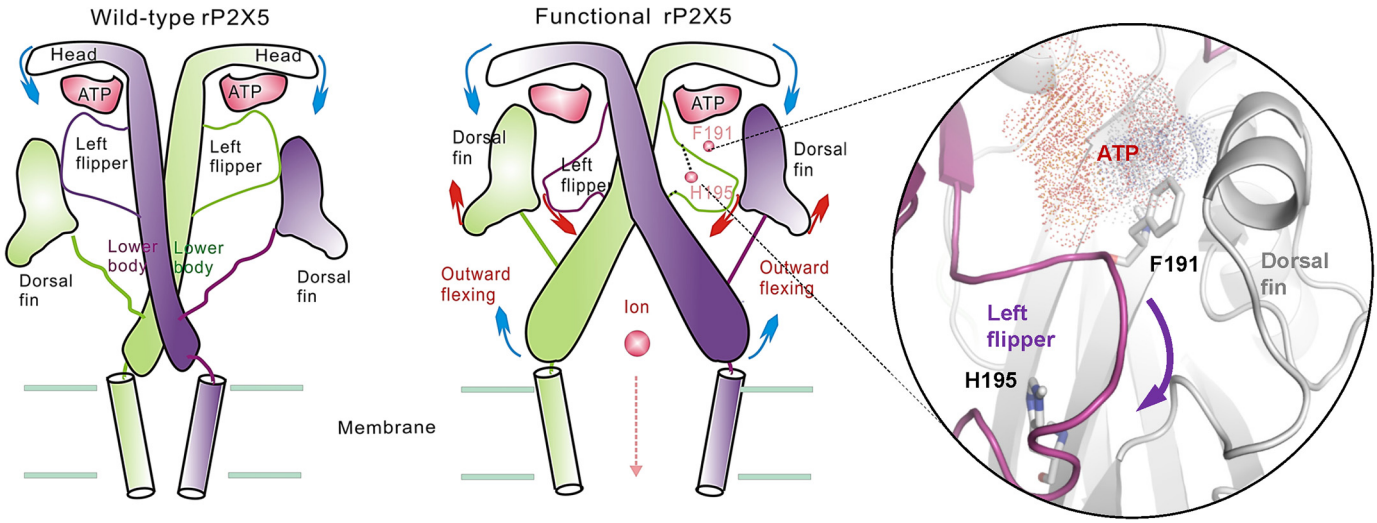

Figure 9. *Schematic* of the mechanism of functional rP2X5 variants. Compared with the negligible sustained subconductance state of $rP2X5^{WT}$, the functional mutants $rP2X5^{S191F}$, $rP2X5^{F195H}$, and $rP2X5^{V67I}$ undergo different conformational changes; when ATP binds to the binding pocket, it repels the LF domain out of the pocket, triggering the conformational changes of other domains, such as the upward motion of the DF domain and the outward flexing of the lower-body domain, finally resulting in the opening of the rP2X5 pore.

F195H substitutions could push the LF domain downward away from the ATP-binding pocket, which consequently increases the channel function of rP2X5, probably by reducing the energy barrier of gating that traps the channel in the subconductance states (Figs. 8 and 9).

Recent advances in the structural determinations of P2X receptors (including P2X3, P2X4, and P2X7) from different species (human, zebrafish, chicken, rat, and panda) have greatly improved our understanding of the molecular mechanism of the P2X gating processes (27–29, 35–37). Previous studies have demonstrated that the relative motions between the LF and DF domains, evoked by bound ATP, are critical for channel gating of P2X4 receptors, whereas impeding this movement can impair or even abolish channel activations (30). Although P2X5 receptors are different from well-investigated P2X4 receptors in many aspects, such as the amino acid sequences, the ATP sensitivity, and current properties, etc. (4), the fact that rP2X5 mutants ($rP2X5^{S191F}$, $rP2X5^{F195H}$, and $rP2X5^{V67I}$) attained enhanced channel function by facilitating the LF conformation switch during the activation suggests a similar role of the LF domain in rP2X5 activation. The saturation mutation study at Ser^{191} showed that only amino acids with the proper size of the side chain at this site could significantly boost channel function of the rP2X5 receptors. Interacting with ATP and further pushing the LF domain outward, Phe^{191} or Tyr^{191} triggers a conformation switch correlated with the channel gating of P2X receptors (30). On the contrary, deprotonation of the side chain of His^{195} abolished its interaction with residues Gly^{292} or Ser^{291} in the LF domain and significantly impaired the channel function restored by F195H. All of these results demonstrate the importance of the allostery of the LF domain in the gating processes of P2X receptors. Because the allostery of the LF domain is critical for the gating processes of both P2X5 and P2X4 receptors (32), it is reasonable to suggest that ATP binding–induced conformational changes of LF domain are also very important for other subtypes of P2X receptors, despite the fact that the sequence of this domain is not very conserved among different subtypes (38).

Among all of the P2X5 receptors reported so far, robust ATP responses were observed in frog P2X5 and chicken P2X5 (39, 40), whereas rat, mouse, and human P2X5 exhibited small ATP-evoked currents (11–14). It seems that the species that appeared later in animal evolution are more likely to exhibit small ATP responses of P2X5. At present, there is no well-accepted explanation for this phenomenon. It is possible that these genes were cloned from organisms at different development stages or that it is simply due to the difference in cloning protocols. Despite the small ATP response of rP2X5, one cannot rule out the possibility that the P2X5 receptor is required for normal physiological functions of these species. Notably, most of the functional P2X5 receptors were cloned from animals in the early developmental stages; for example, the frog P2X5 was cloned from larval amphibian skin (39), and the chicken P2X5 was cloned from embryonic muscle tissues (40). It is possible that functional P2X5 receptors may also be present in rats, mice, and humans at early development stages. In this study, we aimed to determine the mechanism underlying the weak ATP response of rP2X5. Enlightened by the finding that inserting exon 10 of hP2X5 restored the channel function (13, 14), we constructed a series of rP2X5 chimeras and mutants and identified functional rP2X5 variants like $rP2X5^{S191F}$, $rP2X5^{F195H}$, and $rP2X5^{V67I}$. Although the functional variants we reported here may not exist in nature, we cannot rule out the existence of other functional natural rP2X5 variants, which may exert distinct functions in certain populations or under pathological conditions, like the hP2X5-FL (13, 14). Future gene sequencing at the different development stages of those species may be able to clarify this issue.

It is known that ion channel receptors could express both functional and nonfunctional forms at the same or different development stages (41). For example, there are two isoforms of nicotinic acetylcholine receptors (nAChRs), namely embryonic and mature nAChRs. In certain situations, the conversion of embryonic nAChRs to the mature ones is reversible (42). For example, blocking the synaptic activities by cutting off axons or

blocking nAChRs can accelerate the synthesis of new nAChRs. In addition, electric stimulation of the denervated muscle fibers can directly inhibit the synthesis of embryonic nAChRs (43). AMPA receptors can also be classified into two isoforms distinguished by calcium permeability: calcium-permeable (GluR2-Q) and calcium-impermeable (GluR2-R), which differ from each other by a single amino acid (44). Although most reported AMPA receptors are calcium-impermeable, studies have shown that calcium-permeable AMPA receptors play important roles as well. The latter have been associated with the abnormal calcium activity in the early stages of Alzheimer's disease and could be a potential drug target for this disease (45). Our finding that single-residue substitution could switch nonfunctional rP2X5 to functional variants (*e.g.* $rP2X5^{S191F}$, $rP2X5^{F195H}$, and $rP2X5^{V67I}$) raises the possibility that P2X5 might exist in both functional and nonfunctional isoforms at the same or different development stages. However, future studies are needed to conclusively demonstrate this point.

Finally, it is possible that a functional P2X5 receptor with robust ATP response may be harmful to mature animals, and the rP2X5 with weak ATP response may be necessary for normal physiological functions. For example, the P2X5 with weak ATP response can assemble heterogeneously with other functional subtypes (20–25, 46), like P2X1/5 and P2X2/5. Also, the small, sustained ATP response may be involved in the regulation of other ion channels or proteins, such as the ischemic pain induced by P2X5-mediated sensitization of acid-sensing ion channel 3 (ASIC3) during anaerobic exercise (17). Such kinds of interactions have been observed in other P2X subtypes as well. For example, when P2X2 was co-expressed with nAChRs, simultaneous activation of both types of channels produces much smaller currents when compared with currents evoked by activating a single channel type each time, suggesting a direct or indirect interaction between these two channel types (47). Very recently, it was demonstrated that ASIC3 and P2X3 form a pain-relevant cognate receptor (48). The two proteins do not appear to form a heteromeric channel, but they tightly associate with each other to form a protein complex, mediating unidirectional inhibition (48). Thus, P2X5 receptors might exert its role through assembling heterogeneously with other functional P2X subtypes or interacting with other proteins.

In summary, we demonstrate that single-residue substitution can increase the current amplitude of rP2X5 receptors (*e.g.* $rP2X5^{S191F}$, $rP2X5^{F195H}$, and $rP2X5^{V67I}$). Expression of these functional mutants in model animals may provide important information about whether the rP2X5 receptors with weak ATP response are necessary for normal physiological functions and whether the functional variants with robust ATP response, like $rP2X5^{S191F}$, might be harmful to mature animals.

Experimental procedures

Drugs and mutagenesis

Most drugs were purchased from Sigma. The cDNAs of rP2X5 and hP2X5 were kind gifts of Drs. Lin-Hua Jiang, Alan North, and Tian-Le Xu. They were then subcloned into the pEGFP-N1 and/or pCDNA3.0 (with EE-tag) vectors. All mutants were constructed by the QuikChange mutagenesis kit and were verified by DNA sequencing as we described previously (49, 50). The QuikChange mutagenesis kit was also used for inserting a short sequence into the expression construct by carefully designed primers. The exon 10 of hP2X5 is a little bit too long (~60 bp) to be inserted into the target construct through one PCR; therefore, we divided the whole exon 10 sequence into two parts and inserted them into the hP2X5 one by one to finally obtain full-length hP2X5 (hP2X5-FL). For the construction of various chimeras between the hP2X5-FL and rP2X5, ~20–60 bp of rP2X5 were replaced by the identical sequence of hP2X5-FL according to the procedure used in the insertion of exon 10 into hP2X5 above.

Cell culture and electrophysiology

As described previously (32, 51), human embryonic kidney 293 (HEK-293) cells were cultured in conditions containing 88% Dulbecco's modified Eagle's medium, 10% FBS, and antibiotics, and their suitable growth environment was 5% CO_2 and 95% air in a humidified atmosphere at 37 °C. The transfection of plasmids was performed using Hilymax (Dojindo Laboratories, Kumamoto, Japan) according to the manufacturer's protocol.

Whole-cell recordings under the voltage clamp were carried out 24–48 h after transient transfection using Axon 200B at room temperature (23 ± 2 °C). The recording electrodes were filled with pipette solutions, and the resistance was about 3–5 megohms. Membrane currents were measured with a patch-clamp amplifier Axon 200B (Molecular Devices) and low-pass-filtered at 2 kHz. All currents were sampled and processed using a Digitata 1440 interface and a computer operating the Clampex and Clampfit version 14.0 software (Molecular Devices). The standard solution for cell incubating contained 150 mM NaCl, 5 mM KCl, 2 mM $CaCl_2$, 1 mM $MgCl_2$, 10 mM glucose, and 10 mM HEPES, and the pH was modulated to 7.2–7.4. The standard internal solution infused into patch electrodes included 30 mM NaCl, 120 mM KCl, 1 mM $MgCl_2$, 0.5 mM $CaCl_2$, and 5 mM EGTA, and the pH was modulated to 7.2 using Tris-base. During the process of electrophysiological recordings under voltage clamp conditions, the clamp value of membrane potential was set at −60 mV. Drugs were dissolved in external solutions and applied by means of a fast pressure-driven computer-controlled microperfusion system OctaFlow08P (ALA Scientific Instruments). Dose-response curves were obtained from recording a variety of ATP concentrations, the corresponding currents were normalized to the maximum current amplitude, and currents were recorded every 20 min with ~10–20-s ATP application. Single-channel recordings using outside-out configuration were performed 24–48 h after transient transfection at room temperature (23 ± 2 °C). Recording electrodes were drawn from borosilicate glass (World Precision Instruments, Inc.) and polished to produce resistance of about 5–10 megohms. The holding membrane potential was set at −120 mV, and the external and internal solutions are the same as for the whole-cell recording. Single-channel currents were recorded at 50 kHz with a 2-kHz filter and low-pass-filtered at 300 Hz using the AxonPatch 200B amplifier in conjunction with pClamp 14 software (Molecular Devices).

Cell-surface biotinylation and Western blot analysis

Cell-surface biotinylation and Western blotting were carried out according to protocols used previously (30). rP2X5^{WT} or mutants were expressed in HEK-293 cells. These cells were washed with chilled PBS and then bathed in solution containing sulfo-NHS-LC-biotin. This incubation reaction was ceased with glycine (20 mM) dissolved in PBS. Finally, the treated cells were gathered and lysed with radioimmune precipitation assay buffer. 10% of the volume of supernatant was separated and used as total protein fraction. The rest of the biotinylated proteins were attached to NeutrAvidin-linked agarose resin by 3–5-h incubation at 4 °C and then rinsed several times with chilled PBS. These proteins were used as surface proteins. All proteins were boiled with SDS-loading buffer for 5 min at 95°C with 1% β-ME (for reducing experiments) or not (for nonreducing experiments). These proteins were analyzed by SDS-PAGE. With an 8–10% separation gel and a 4% stacking gel, these samples were separated and then transferred to a polyvinylidene difluoride membrane. The polyvinylidene difluoride membrane was blocked with 5% milk dissolved in PBS at room temperature for 1–2 h and then incubated overnight at 4 °C with anti-EGFP tag (1:1,000; Roche Applied Science), anti-EE tag (1:1,000; Cell Signaling Technology), or anti-GAPDH (1:2,000; Sungene Biotech) antibodies diluted with 5% milk as ratio shown above. The membrane was further incubated with HRP-conjugated secondary antibodies for EGFP tag (25 °C, 1 h, 1:1,000; goat anti-rabbit IgG(HL)-HRP; Sungene Biotech) or GAPDH (25 °C, 1 h, 1:3,000; goat anti-mouse IgG(HL)-HRP; Sungene Biotech), and finally visualized by exposure with the ImageQuant RT ECL system (GE Healthcare) for 1–3 min by means of ECL solution (Thermo Fisher Scientific). Analysis of protein expression was repeated by at least three independent experiments.

Homology modeling

As described previously (52), program Modeler 9.9 (53) was used to create homology models of rP2X5 and its mutants on the basis of the crystal structures of zfP2X4 receptors in closed (Protein Data Bank code 4DW0) and open (Protein Data Bank code 4DW1) states (27, 28). The alignment of sequence was ordered and adjusted according to the published alignment (27). The raw models were further optimized and minimized by using the OPLS_2005 force field. Finally, the program ProCheck (54) was used to verify those deeply processing models.

MD simulations

As described previously (30, 31, 55), the program DESMOND (56) was used to perform all MD simulations with a constant number of particles, pressure (1 bar), and temperature (300 K) and periodic boundary conditions, which use a particular "neutral territory" method called the midpoint method to efficiently exploit a high degree of computational parallelism. A default OPLS_2005 force field together with the functional form of the OPLS-AA family of force fields were used for the P2X5 and ATP molecules. The starting structures for MD simulations were energy-minimized by DESMOND. A suitable membrane system in which the transmembrane domain of the rP2X5 might be buried was generated with a large constructed 1-palmitoyl-2-oleoylphosphatidylcholine bilayer, this system was subsequently deposited in simple point charge water molecules. The subsequent addition of counter ions made up for the net negative charge of the system. NaCl (150 mM) was thrown into a simulation box that represents background salt at physiologic conditions. All of the MD simulations ran the DAWNING TC2600 system. Preparation, analysis, and visualization were executed on a DELL T7500 graphic workstation. In light of protocols we used previously (31, 55), the distance and dihedral angle among the atoms were analyzed using the simulation event analysis (SEA) module of Desmond; the r.m.s. fluctuation analysis of protein and ligand and interaction analysis between ATP and rP2X5 (WT and mutated receptors) were carried out in the simulation interaction diagram (SID) module; the pair distributions of the COM among various domains during MD simulations were performed in the radial distribution function module of Desmond.

Data analysis

All results are expressed as mean ± S.D. Statistical comparisons were made using the value of *t* test, pair *t* test, or one-way ANOVA as a standard, where $p < 0.05$ (*) or $p < 0.01$ (**) was considered significant. Concentration-response relationships for ATP activation of WT or mutated channels were obtained by measuring currents activated by different ATP concentrations, and data were collected from 3–8 cells. Current collected from various ATP concentrations was normalized by the maximal current; these data then were fitted to the Hill equation, $I/I_{max} = 1/(1(EC_{50}/[ATP])^n)$, where I is the normalized current at a given concentration of ATP, I_{max} is the maximum normalized current, EC_{50} is the concentration of ATP yielding a current that is half of the maximum, and n is the Hill coefficient.

Author contributions—L.-F. S., Y. L., J. W., L.-D. H., Y. Yang, C.-R. G., and Y. Yu data curation; L.-F. S., Y. L., J. W., X.-Y. C., M. X. Z., H. L., and Y. Yu formal analysis; L.-F. S., J. W., and Y. Yu validation; L.-F. S., J. W., M. X. Z., and Y. Yu visualization; L.-F. S., Y. Yang, X.-Y. C., and M. X. Z. writing-original draft; J. W., H.-S. W., C.-R. G., and Y. Yu funding acquisition; X.-Y. C., Y.-Z. F., Y. T., and Y. Yu writing-review and editing; Y.-Z. F., Y. T., and Y. Yu conceptualization; H. L., H.-S. W., C.-R. G., and Y. Yu supervision; Y. T. resources; Y. Yu investigation.

Acknowledgments—We thank Drs. Lin-Hua Jiang, Alan North, and Tian-Le Xu for kind gifts of the cDNAs of rP2X5 and hP2X5.

References

1. Surprenant, A., and North, R. A. (2009) Signaling at purinergic P2X receptors. *Annu. Rev. Physiol.* **71,** 333–359 CrossRef Medline
2. Idzko, M., Ferrari, D., and Eltzschig, H. K. (2014) Nucleotide signalling during inflammation. *Nature* **509,** 310–317 CrossRef Medline
3. Khakh, B. S., and North, R. A. (2006) P2X receptors as cell-surface ATP sensors in health and disease. *Nature* **442,** 527–532 CrossRef Medline
4. North, R. A. (2002) Molecular physiology of P2X receptors. *Physiol. Rev.* **82,** 1013–1067 CrossRef Medline
5. Coddou, C., Yan, Z., Obsil, T., Huidobro-Toro, J. P., and Stojilkovic, S. S. (2011) Activation and regulation of purinergic P2X receptor channels. *Pharmacol. Rev.* **63,** 641–683 CrossRef Medline
6. Abdulqawi, R., Dockry, R., Holt, K., Layton, G., McCarthy, B. G., Ford, A. P., and Smith, J. A. (2015) P2X3 receptor antagonist (AF-219) in refrac-

tory chronic cough: a randomised, double-blind, placebo-controlled phase 2 study. *Lancet* **385,** 1198–1205 CrossRef Medline
7. Stock, T. C., Bloom, B. J., Wei, N., Ishaq, S., Park, W., Wang, X., Gupta, P., and Mebus, C. A. (2012) Efficacy and safety of CE-224,535, an antagonist of P2X7 receptor, in treatment of patients with rheumatoid arthritis inadequately controlled by methotrexate. *J. Rheumatol.* **39,** 720–727 CrossRef Medline
8. Bo, X., Zhang, Y., Nassar, M., Burnstock, G., and Schoepfer, R. (1995) A P2X purinoceptor cDNA conferring a novel pharmacological profile. *FEBS Lett.* **375,** 129–133 CrossRef Medline
9. Brake, A. J., Wagenbach, M. J., and Julius, D. (1994) New structural motif for ligand-gated ion channels defined by an ionotropic ATP receptor. *Nature* **371,** 519–523 CrossRef Medline
10. Chen, C. C., Akopian, A. N., Sivilotti, L., Colquhoun, D., Burnstock, G., and Wood, J. N. (1995) A P2X purinoceptor expressed by a subset of sensory neurons. *Nature* **377,** 428–431 CrossRef Medline
11. Collo, G., North, R. A., Kawashima, E., Merlo-Pich, E., Neidhart, S., Surprenant, A., and Buell, G. (1996) Cloning of P2X5 and P2X6 receptors and the distribution and properties of an extended family of ATP-gated ion channels. *J. Neurosci.* **16,** 2495–2507 CrossRef Medline
12. Cox, J. A., Barmina, O., and Voigt, M. M. (2001) Gene structure, chromosomal localization, cDNA cloning and expression of the mouse ATP-gated ionotropic receptor P2X5 subunit. *Gene* **270,** 145–152 CrossRef Medline
13. Bo, X., Jiang, L. H., Wilson, H. L., Kim, M., Burnstock, G., Surprenant, A., and North, R. A. (2003) Pharmacological and biophysical properties of the human P2X5 receptor. *Mol. Pharmacol.* **63,** 1407–1416 CrossRef Medline
14. Kotnis, S., Bingham, B., Vasilyev, D. V., Miller, S. W., Bai, Y., Yeola, S., Chanda, P. K., Bowlby, M. R., Kaftan, E. J., Samad, T. A., and Whiteside, G. T. (2010) Genetic and functional analysis of human P2X5 reveals a distinct pattern of exon 10 polymorphism with predominant expression of the nonfunctional receptor isoform. *Mol. Pharmacol.* **77,** 953–960 CrossRef Medline
15. Vannier, B., Peyton, M., Boulay, G., Brown, D., Qin, N., Jiang, M., Zhu, X., and Birnbaumer, L. (1999) Mouse trp2, the homologue of the human trpc2 pseudogene, encodes mTrp2, a store depletion-activated capacitative Ca^{2+} entry channel. *Proc. Natl. Acad. Sci. U.S.A.* **96,** 2060–2064 CrossRef Medline
16. Ryten, M., Dunn, P. M., Neary, J. T., and Burnstock, G. (2002) ATP regulates the differentiation of mammalian skeletal muscle by activation of a P2X5 receptor on satellite cells. *J. Cell Biol.* **158,** 345–355 CrossRef Medline
17. Birdsong, W. T., Fierro, L., Williams, F. G., Spelta, V., Naves, L. A., Knowles, M., Marsh-Haffner, J., Adelman, J. P., Almers, W., Elde, R. P., and McCleskey, E. W. (2010) Sensing muscle ischemia: coincident detection of acid and ATP via interplay of two ion channels. *Neuron* **68,** 739–749 CrossRef Medline
18. Schwiebert, E. M., and Kishore, B. K. (2001) Extracellular nucleotide signaling along the renal epithelium. *Am. J. Physiol. Renal Physiol.* **280,** F945–F963 CrossRef Medline
19. Gröschel-Stewart, U., Bardini, M., Robson, T., and Burnstock, G. (1999) Localisation of P2X5 and P2X7 receptors by immunohistochemistry in rat stratified squamous epithelia. *Cell Tissue Res.* **296,** 599–605 CrossRef Medline
20. Saul, A., Hausmann, R., Kless, A., and Nicke, A. (2013) Heteromeric assembly of P2X subunits. *Front. Cell Neurosci.* **7,** 250 CrossRef Medline
21. Surprenant, A., Schneider, D. A., Wilson, H. L., Galligan, J. J., and North, R. A. (2000) Functional properties of heteromeric P2X(1/5) receptors expressed in HEK cells and excitatory junction potentials in guinea-pig submucosal arterioles. *J. Auton. Nerv. Syst.* **81,** 249–263 CrossRef Medline
22. Lê, K. T., Boué-Grabot, E., Archambault, V., and Séguéla, P. (1999) Functional and biochemical evidence for heteromeric ATP-gated channels composed of P2X1 and P2X5 subunits. *J. Biol. Chem.* **274,** 15415–15419 CrossRef Medline
23. Chen, L., Liu, Y. W., Yue, K., Ru, Q., Xiong, Q., Ma, B. M., Tian, X., and Li, C. Y. (2016) Differential expression of ATP-gated P2X receptors in DRG between chronic neuropathic pain and visceralgia rat models. *Purinergic Signal.* **12,** 79–87 CrossRef Medline
24. Palygin, O., Lalo, U., Verkhratsky, A., and Pankratov, Y. (2010) Ionotropic NMDA and P2X1/5 receptors mediate synaptically induced Ca^{2+} signalling in cortical astrocytes. *Cell Calcium* **48,** 225–231 CrossRef Medline
25. Compan, V., Ulmann, L., Stelmashenko, O., Chemin, J., Chaumont, S., and Rassendren, F. (2012) P2X2 and P2X5 subunits define a new heteromeric receptor with P2X7-like properties. *J. Neurosci.* **32,** 4284–4296 CrossRef Medline
26. Lê, K. T., Paquet, M., Nouel, D., Babinski, K., and Séguéla, P. (1997) Primary structure and expression of a naturally truncated human P2X ATP receptor subunit from brain and immune system. *FEBS Lett.* **418,** 195–199 CrossRef Medline
27. Kawate, T., Michel, J. C., Birdsong, W. T., and Gouaux, E. (2009) Crystal structure of the ATP-gated P2X(4) ion channel in the closed state. *Nature* **460,** 592–598 CrossRef Medline
28. Hattori, M., and Gouaux, E. (2012) Molecular mechanism of ATP binding and ion channel activation in P2X receptors. *Nature* **485,** 207–212 CrossRef Medline
29. Mansoor, S. E., Lü, W., Oosterheert, W., Shekhar, M., Tajkhorshid, E., and Gouaux, E. (2016) X-ray structures define human P2X(3) receptor gating cycle and antagonist action. *Nature* **538,** 66–71 CrossRef Medline
30. Zhao, W. S., Wang, J., Ma, X. J., Yang, Y., Liu, Y., Huang, L. D., Fan, Y. Z., Cheng, X. Y., Chen, H. Z., Wang, R., and Yu, Y. (2014) Relative motions between left flipper and dorsal fin domains favour P2X4 receptor activation. *Nat. Commun.* **5,** 4189 CrossRef Medline
31. Wang, J., Wang, Y., Cui, W. W., Huang, Y., Yang, Y., Liu, Y., Zhao, W. S., Cheng, X. Y., Sun, W. S., Cao, P., Zhu, M. X., Wang, R., Hattori, M., and Yu, Y. (2018) Druggable negative allosteric site of P2X3 receptors. *Proc. Natl. Acad. Sci. U.S.A.* **115,** 4939–4944 CrossRef Medline
32. Wang, J., Sun, L. F., Cui, W. W., Zhao, W. S., Ma, X. F., Li, B., Liu, Y., Yang, Y., Hu, Y. M., Huang, L. D., Cheng, X. Y., Li, L., Lu, X. Y., Tian, Y., and Yu, Y. (2017) Intersubunit physical couplings fostered by the left flipper domain facilitate channel opening of P2X4 receptors. *J. Biol. Chem.* **292,** 7619–7635 CrossRef Medline
33. Cremlyn, R. J. (1996) *An Introduction to Organosulfur Chemistry*, pp. 7–15, Wiley, New York
34. Samways, D. S., Khakh, B. S., Dutertre, S., and Egan, T. M. (2011) Preferential use of unobstructed lateral portals as the access route to the pore of human ATP-gated ion channels (P2X receptors). *Proc. Natl. Acad. Sci. U.S.A.* **108,** 13800–13805 CrossRef Medline
35. Kasuya, G., Yamaura, T., Ma, X. B., Nakamura, R., Takemoto, M., Nagumo, H., Tanaka, E., Dohmae, N., Nakane, T., Yu, Y., Ishitani, R., Matsuzaki, O., Hattori, M., and Nureki, O. (2017) Structural insights into the competitive inhibition of the ATP-gated P2X receptor channel. *Nat. Commun.* **8,** 876 CrossRef Medline
36. Karasawa, A., and Kawate, T. (2016) Structural basis for subtype-specific inhibition of the P2X7 receptor. *eLife* **5,** e22153 CrossRef Medline
37. McCarthy, A. E., Yoshioka, C., and Mansoor, S. E. (2019) Full-length P2X7 structures reveal how palmitoylation prevents channel desensitization. *Cell* **179,** 659–670.e13 CrossRef Medline
38. Wang, J., and Yu, Y. (2016) Insights into the channel gating of P2X receptors from structures, dynamics and small molecules. *Acta Pharmacol. Sin.* **37,** 44–55 CrossRef Medline
39. Jensik, P. J., Holbird, D., Collard, M. W., and Cox, T. C. (2001) Cloning and characterization of a functional P2X receptor from larval bullfrog skin. *Am. J. Physiol. Cell Physiol.* **281,** C954–C962 CrossRef Medline
40. Meyer, M. P., Gröschel-Stewart, U., Robson, T., and Burnstock, G. (1999) Expression of two ATP-gated ion channels, P2X5 and P2X6, in developing chick skeletal muscle. *Dev. Dyn.* **216,** 442–449 CrossRef Medline
41. Geuder, K. I., Marx, A., Witzemann, V., Schalke, B., Toyka, K., Kirchner, T., and Müller-Hermelink, H.-K. (1992) Pathogenetic significance of fetal-type acetylcholine receptors on thymic myoid cells in myasthenia gravis. *Dev. Immunol.* **2,** 69–75 CrossRef Medline
42. Bouzat, C., Bren, N., and Sine, S. M. (1994) Structural basis of the different gating kinetics of fetal and adult acetylcholine receptors. *Neuron* **13,** 1395–1402 CrossRef Medline
43. Adams, L., Carlson, B. M., Henderson, L., and Goldman, D. (1995) Adaptation of nicotinic acetylcholine receptor, myogenin, and MRF4 gene ex-

pression to long-term muscle denervation. *J. Cell Biol.* **131,** 1341–1349 CrossRef Medline

44. Burnashev, N., Monyer, H., Seeburg, P. H., and Sakmann, B. (1992) Divalent ion permeability of AMPA receptor channels is dominated by the edited form of a single subunit. *Neuron* **8,** 189–198 CrossRef Medline
45. Chang, E. H., Savage, M. J., Flood, D. G., Thomas, J. M., Levy, R. B., Mahadomrongkul, V., Shirao, T., Aoki, C., and Huerta, P. T. (2006) AMPA receptor downscaling at the onset of Alzheimer's disease pathology in double knockin mice. *Proc. Natl. Acad. Sci. U.S.A.* **103,** 3410–3415 CrossRef Medline
46. Verkhratsky, A., and Burnstock, G. (2014) Purinergic and glutamatergic receptors on astroglia. *Adv. Neurobiol.* **11,** 55–79 CrossRef Medline
47. Khakh, B. S., Zhou, X., Sydes, J., Galligan, J. J., and Lester, H. A. (2000) State-dependent cross-inhibition between transmitter-gated cation channels. *Nature* **406,** 405–410 CrossRef Medline
48. Stephan, G., Huang, L., Tang, Y., Vilotti, S., Fabbretti, E., Yu, Y., Nörenberg, W., Franke, H., Gölöncsér, F., Sperlágh, B., Dopychai, A., Hausmann, R., Schmalzing, G., Rubini, P., and Illes, P. (2018) The ASIC3/P2X3 cognate receptor is a pain-relevant and ligand-gated cationic channel. *Nat. Commun.* **9,** 1354 CrossRef Medline
49. Zhao, W. S., Sun, M. Y., Sun, L. F., Liu, Y., Yang, Y., Huang, L. D., Fan, Y. Z., Cheng, X. Y., Cao, P., Hu, Y. M., Li, L., Tian, Y., Wang, R., and Yu, Y. (2016) A highly conserved salt bridge stabilizes the kinked conformation of β2,3-sheet essential for channel function of P2X4 receptors. *J. Biol. Chem.* **291,** 7990–8003 CrossRef Medline
50. Yang, X. N., Niu, Y. Y., Liu, Y., Yang, Y., Wang, J., Cheng, X. Y., Liang, H., Wang, H. S., Hu, Y. M., Lu, X. Y., Zhu, M. X., Xu, T. L., Tian, Y., and Yu, Y. (2017) The nonproton ligand of acid-sensing ion channel 3 activates mollusk-specific FaNaC channels via a mechanism independent of the native FMRFamide peptide. *J. Biol. Chem.* **292,** 21662–21675 CrossRef Medline
51. Niu, Y. Y., Yang, Y., Liu, Y., Huang, L. D., Yang, X. N., Fan, Y. Z., Cheng, X. Y., Cao, P., Hu, Y. M., Li, L., Lu, X. Y., Tian, Y., and Yu, Y. (2016) Exploration of the peptide recognition of an amiloride-sensitive FMRFamide peptide-gated sodium channel. *J. Biol. Chem.* **291,** 7571–7582 CrossRef Medline
52. Li, B., Wang, J., Cheng, X., Liu, Y., Yang, Y., Yang, X., Guo, C., Niu, Y., Cao, P., Lu, X., Zhu, M. X., Tian, Y., and Yu, Y. (2018) Molecular mechanism underlying the subtype-selectivity of competitive inhibitor NF110 and its distinct potencies in human and rat P2X3 receptors. *Sci. Bull.* **63,** 1616–1625 CrossRef
53. Sali, A., and Blundell, T. L. (1993) Comparative protein modelling by satisfaction of spatial restraints. *J. Mol. Biol.* **234,** 779–815 CrossRef Medline
54. Laskowski, R. A., MacArthur, M. W., Moss, D. S., and Thornton, J. M. (1993) PROCHECK: a program to check the stereochemical quality of protein structures. *J. Appl. Crystallogr.* **26,** 283–291 CrossRef
55. Huang, L. D., Fan, Y. Z., Tian, Y., Yang, Y., Liu, Y., Wang, J., Zhao, W. S., Zhou, W. C., Cheng, X. Y., Cao, P., Lu, X. Y., and Yu, Y. (2014) Inherent dynamics of head domain correlates with ATP-recognition of P2X4 receptors: insights gained from molecular simulations. *PLoS One* **9,** e97528 CrossRef Medline
56. Shaw, D. E. (2005) A fast, scalable method for the parallel evaluation of distance-limited pairwise particle interactions. *J. Comput. Chem.* **26,** 1318–1328 CrossRef Medline